Journal of Hazardous Materials 401 (2021) 123348

Contents lists available at ScienceDirect

Journal of Hazardous Materials

journal homepage: www.elsevier.com/locate/jhazmat

Metal-incorporated mesoporous oxides: Synthesis and applications

Bishnu Prasad Bastakoti[a,*], Debasish Kuila[a], Carlos Salomon[b], Muxina Konarova[c], Miharu Eguchi[c,d], Jongbeom Na[c,d], Yusuke Yamauchi[c,d,e,f]

[a] Department of Chemistry, Applied Sciences & Technology, North Carolina Agricultural and Technical State University, Greensboro, NC 27411, USA
[b] Exosome Biology Laboratory, Centre for Clinical Diagnostics, University of Queensland Centre for Clinical Research, Royal Brisbane and Women's Hospital, The University of Queensland, Brisbane, Queensland, Australia
[c] Australian Institute for Bioengineering and Nanotechnology (AIBN), The University of Queensland, Brisbane, Queensland 4072, Australia
[d] International Research Center for Materials Nanoarchitechtonics (WPI-MANA), National Institute for Materials Science (NIMS), 1-1 Namiki, Tsukuba, Ibaraki 305-0044, Japan
[e] School of Chemical Engineering, The University of Queensland, Brisbane, Queensland 4072, Australia
[f] Department of Plant and Environmental New Resources, Kyung Hee University, 1732 Deogyeong-daero, Giheung-gu, Yongin-si, Gyeonggi-do 446-701, South Korea

GRAPHICAL ABSTRACT

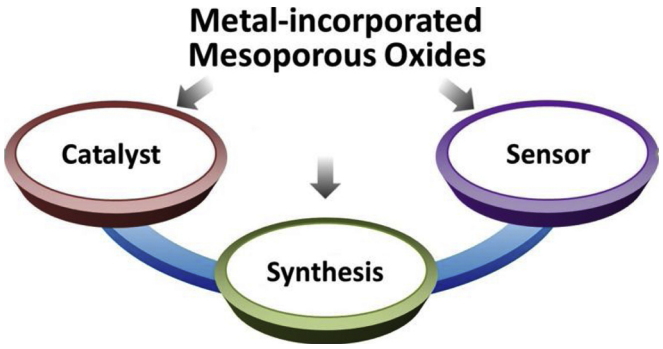

ARTICLE INFO

Editor: Rinklebe Jörg

Keywords:
Mesoporous oxides
Sensors
Catalysts
Environmental remediation
Material design

ABSTRACT

Mesoporous oxides are outstanding metal nanoparticle catalyst supports owing to their well-defined porous structures. Such mesoporous architectures not only prevent the aggregation of metal nanoparticles but also enhance their catalytic performance. Metal/metal oxide heterojunctions exhibit unique chemical and physical properties because of the surface reconstruction around the junction and electron transfer/interaction across the interface. This article reviews the methods used for synthesizing metal-supported hybrid nanostructures and their applications as catalysts for environmental remediation and sensors for detecting hazardous materials.

1. Introduction

Over the past few years, metal nanoparticles have gained considerable interest for catalytic applications owing to their unique properties including high surface area and well-controlled facets (Zhang and Wang, 2014; Skrabalak and Xia, 2009; Sun and Xia, 2002; Rodrigues et al., 2019). Au, Pt, Pd, Ru, Ni, and Co and their binary, tertiary, and quaternary compositions have been extensively investigated for a wide range of catalytic applications (Au et al., 1998; Wong et al., 2011; Ito et al., 2014). As compared to bulk catalysts,

* Corresponding author.
E-mail address: bpbastakoti@ncat.edu (B.P. Bastakoti).

https://doi.org/10.1016/j.jhazmat.2020.123348
Received 15 April 2020; Received in revised form 24 June 2020; Accepted 27 June 2020
Available online 30 June 2020
0304-3894/ Published by Elsevier B.V.

nanocatalysts significantly reduce the process cost and time (Shan et al., 2019; Ran et al., 2018; Song et al., 2015; Yan et al., 2015; Ray and Pal, 2017). The catalytic activity and selectivity of colloidal metal nanoparticles depend on their shape, size, and support material (Decarolis et al., 2018; Lin and Compton, 2017).

Chemical reduction and thermal decomposition based on colloidal chemistry are the most widely used methods for the synthesis of metal nanoparticles. Atomically clean metal nanoparticles are ideal for characterizing their surface properties. However, it is not possible to generate such nanoparticles in a chemical flask. Metal nanoparticles with clean surfaces can only be obtained under high vacuum conditions. Furthermore, as bare nanoparticles are kinetically as well as thermodynamically unstable, they always show a tendency to lower their high surface energy either by sorption of molecules from the surroundings or *via* aggregation. Steric and/or electrostatic stabilization forces are normally used to prevent the aggregation of nanoparticles (Tadros, 2012). Incorporation or encapsulation (in certain cases) of nanoparticles in solid porous substrates is a commonly used approach for the preparation of nanocatalysts and their subsequent applications (Genna et al., 2013; Jin et al., 2012a, b). The porous substrate not only stabilizes the nanoparticles but also induces a synergistic effect in many applications (Yang et al., 2017; Plata et al., 2016; Muller et al., 2018).

Different mesoporous materials have been developed as nanoparticle supports in the past few years owing to their optimum pore sizes (2–50 nm), high surface areas, and easy and reliable synthesis methods (Yanagisawa et al., 1990; Kresge et al., 1992; Bastakoti et al., 2015a). These properties of mesoporous materials make them promising candidates for applications such as catalysis, sensing, drug delivery, and gas separation (Li et al., 2014). In general, mesoporous metal oxides with different compositions are synthesized using either soft (surfactants, block copolymers, *etc*.) or hard (SBA-15, MCM-48, MCM-41, CMK-1, CMK-3, *etc*.) templates (Gu and Schüth, 2014; Li et al., 2016; Zhang et al., 2019a; Wang et al., 2011; Morris et al., 2008; Xu et al., 2020). Mesoporous metal oxides exhibit intrinsic catalytic functionalities. In addition, they can be used as supports for metal nanocatalysts. The numerous openings in the mesopores of these metal oxides facilitate the encapsulation of small metal nanoparticles and provide easy access to gases and other molecules. The catalytic activity, selectivity, and stability of mesoporous metal oxide-supported nanoparticle catalysts depend on the physicochemical properties of the metal nanoparticles and mesoporous supports and the interactions between them (Shan et al., 2019; Zheng et al., 2019; Jo et al., 2018; Gates et al., 2017; Ghimire et al., 2019; Goncalves and Jaroniec, 2019). Thus, designing optimum nanoarchitectures for metal nanocatalysts is a topic of interest for researchers. In order to develop optimum metal supported nanoarchitectures at the nanoscale level, it is imperative to understand the synthesis methodology, the mode of interaction between the support and metal nanoparticles, and the potential applications of the resulting nanoarchitectures. This review discusses several important environmental as well as other related applications of metal-incorporated mesoporous oxides.

2. Interaction of metal nanoparticles with mesoporous oxides

For a long time, it was assumed that mesoporous oxides act as inert supports to stabilize the incorporated nanoparticles. This concept has changed over the years as the small metal nanoparticles that adhered to supporting oxides exhibited remarkable performance for different applications (Xu et al., 2020). For example, owing to the interaction of platinum nanoparticles with mesoporous transition metal oxides at the interface, the rate of the oxidation of CO is significantly enhanced (An et al., 2013a). Therefore, understanding the interaction between metal nanoparticles and mesoporous metal oxides is crucial for developing metal-incorporated mesoporous oxides with desired properties or applications (van Deelen et al., 2019; Oh et al., 2018; Yuan et al., 2010; Ro et al., 2018; Witzke et al., 2017). The complexity of these interactions reflects the complexity of the metal/metal oxide interface (Caldas et al., 2017). The same metal can behave very differently depending upon its interaction with the support materials. The interfacial energy arising from the interactions between the metal nanoparticles and support is affected by the size and orientation of the nanoparticles (Kale and Christopher, 2016; Shekhar et al., 2012; Winterbo, 1967; Cargnello et al., 2013; Campbell et al., 2002). The coordination environment of the exposed metal atoms is a function of the particle size. The relative fraction of exposed atoms existing in different local environments varies as the dimensions of the supported metal particle decreases (Ro et al., 2018).

From electronic and geometric perspectives, metal oxides are more complicated than metals. The electronic and geometric properties of metal oxides can be tailored by doping them with different atoms or ions. The properties of doped metal oxide-supported metals depend on the electron exchange between the dopants and the metal oxides (Stavale et al., 2012). When metal atoms or clusters interact with the metal oxide support having anion vacancies (defects), the charge transfer occurs from the support to the adsorbed metal. The defects occupy higher energy levels in the bandgap and can be located above the Fermi level of the deposited metal nanoparticle, thus inducing the electron flow (Lohaus et al., 2018). Stavale et al. investigated the effects of metal dopants on the properties of alkaline earth metal oxide supports. Cr and Mo (group 6 elements) have been incorporated into the rock salt oxides of MgO and CaO, respectively (Fig. 1a) (Stavale et al., 2012). The Au binding behaviors of MgO and CaO have been investigated to demonstrate the charge transfer in them. Mo^{3+} ions incorporated into CaO can donate an electron to the surface of Au atoms. However, in MgO-Cr, the Cr^{3+} ions cannot be oxidized any further, which inhibits the electron transfer to the Au atoms (Fig. 1b) (Stavale et al., 2012). This difference in the characteristics of MgO-Cr and CaO-Mo can be attributed to the characteristics of the dopants rather than those of the oxides. The Mo^{3+} ions in CaO-Mo oxidize into Mo^{4+} by donating an electron. In contrast, in the case of MgO-Cr, the Cr^{3+} ions replace the Mg^{2+} ions, leading to the formation of cation vacancies to maintain the electroneutrality of the compound (Stavale et al., 2012; Pacchioni and Freund, 2018).

The catalytic activity of metal-incorporated metal oxides also depends on the nature of the metal oxide support. For example, alumina- and magnesia-supported Au nanoparticles are more active than silica-supported Au nanoparticles (Bond and Thompson, 1999). Oxide supports can be classified into non-reducible (Al_2O_3, SiO_2, MgO, *etc*.) and reducible (TiO_2, CeO_2, NiO, WO_3, *etc*.) oxides (Pacchioni and Freund, 2018; Barcaro and Fortunelli, 2019). The binding properties of these two groups of oxides are completely different. In general, non-reducible oxides have high-energy conduction band and low-energy valence band, and thus exhibit low reactivity. Hence, these oxides act as inert supports in catalysis. However, these properties change drastically when the size of the oxides reduces to the nanoscale. Non-reducible oxides exhibit steps, kinks, and corners, which affect the electronic properties of the oxides by introducing new acceptor and donor levels (Pacchioni et al., 1994). Generation of defects favors the charge transfer from the metal nanoparticles to the oxide (Pacchioni and Freund, 2018). The oxygen anions of reducible metal oxides show some oxidizing power. The oxide/metal interface is the most active catalytic site in these materials and is referred to as the hot-spot zone (Rodriguez et al., 2009). Owing to their electron donating properties, metal nanoparticles induce the formation of vacancies in metal-supported structures (Vayssilov et al., 2011).

Metal-oxide interactions can be supported by experimental proofs as well as speculations (Guo et al., 2015). Libuda and coworkers found that in ceria-supported Pt nanoparticles, the oxidative metal-oxide interaction occurs via electron transfer from the Pt nanoparticles to the support (ceria) and oxygen transfer from ceria to Pt (Vayssilov et al., 2011). The chemisorption of active metal nanoparticles on oxide surfaces induces charge transfer, which improves the rate of the catalytic

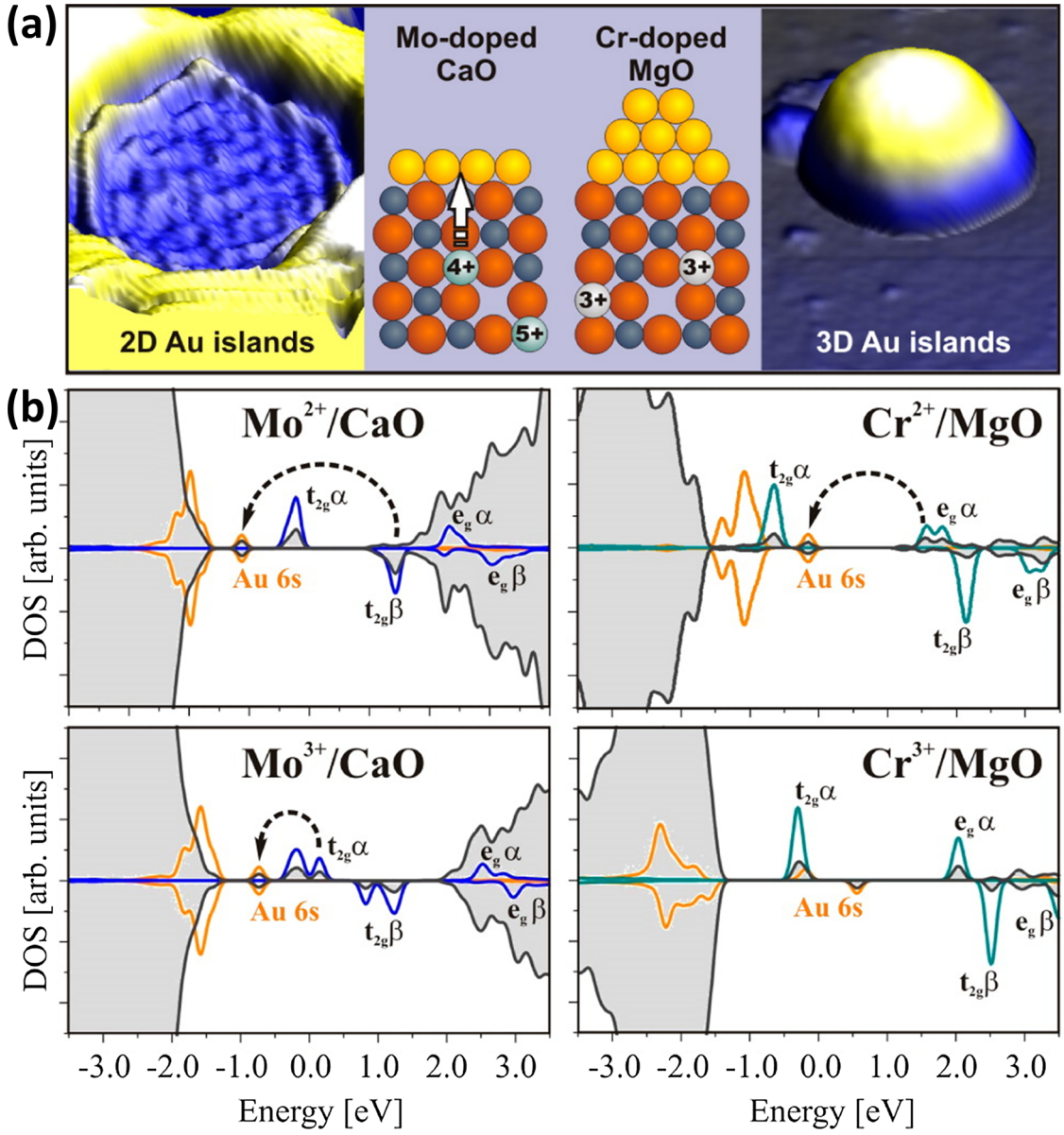

Fig. 1. (a) Scanning tunneling microscopy images of Mo-doped CaO and Cr-doped MgO films. (b) Projected densities of states for CaO-Mo and MgO-Cr in the presence of Au atoms calculated for two different charge states of the transition metal ions. Charge transfer from the highest occupied molecular orbital of the dopant to the Au 6s affinity levels is indicated by arrows. Reprinted with permission (Stavale et al., 2012). Copyright 2013, American Chemical Society.

reaction. The lattice mismatch between the metal nanoparticles and metal oxide surface causes the contraction or expansion of the lattice, which improves the inter-facial bonding stability of the catalyst (Tauster et al., 1978). The adhesion energy between a metal and metal oxide creates a repulsive interaction between the neighboring metal nanoparticles. Such repulsion acts as an activation barrier to prevent the adjacent metal nanoparticles from diffusing together and agglomerating, thus inhibiting the catalyst sintering (Farmer and Campbell, 2010).

3. Synthesis of metal-incorporated mesoporous oxides

Various synthetic routes have been reported for metal-incorporated mesoporous oxides. Depending on the mode of nanoparticle encapsulation, metal-incorporated mesoporous oxides are mainly synthesized using pre-synthesized nanoparticles and via the impregnation-reduction and one-pot synthesis methods. Metal nanoparticles are also used to form the core of core-shell or yolk-shell nanoparticles with nanoporous oxides as the shells (Chaudhuri and Paria, 2012; Gawande et al., 2015; Li et al., 2019; Yang et al., 2015; Talebzadeh et al., 2019; Bastakoti et al., 2012). Core-shell nanoparticles comprise of two or more materials. The choice of the core and shell materials mainly depends on the application (Cai et al., 2009; Tao et al., 2008; Lim et al., 2016; Zhong et al., 2018). The yolk-shell structure is a special variant of the core-shell structure, in which the core (yolk) is free to move into the hollow interior of the shell. Core-shell and yolk-shell materials can accommodate a large number of molecules in their void space, which makes them suitable for nanoreactor (Lin and Doong, 2017) and payload delivery applications (Shen et al., 2017).

3.1. Using pre-synthesized metal nanoparticles

Pre-synthesized metal nanoparticles can be encapsulated into the mesopores of metal oxides via the reduction of metal ions in the solution or a sol-gel reaction. Metal nanoparticles are mainly prepared via a colloidal synthesis method with appropriate functionalization.

Reducing agents such as sodium borohydride, ascorbic acid, and hydrazine are used to reduce metal ions in the solution, while capping agents such as polyvinylpyrrolidone (PVP), thiols, and surfactants are used to prevent nanoparticle aggregation (Bastús et al., 2014; Schrade et al., 2013; Niu and Li, 2014; Barman et al., 2018). Preformed PVP capped metal nanoparticles are mixed with the polymer solution followed by the addition of the metal oxide precursors. Nucleation and inorganic-organic co-assembly stabilize the size of the resulting metal nanoparticles in the nanoscale range. The polymer-assisted method is used to synthesize nanomaterials with shape control (Zhang et al., 2020a). Different types of polymers such as homopolymers (Parra and Haque, 2015) and double hydrophilic (Bastakoti et al., 2012; Guragain et al., 2018) and amphiphilic block copolymers (Li et al., 2016; Bastakoti et al., 2011) are employed as adjustable masks for the synthesis of nanoparticles. The polymer layer on the nanoparticles undergoes transformation during the crystal growth. The nanoparticles prepared using this approach are highly resistant to aggregation but at the same time are fluidic and adjustable to control the crystal growth (Wang et al., 2018).

Photoreduction has been investigated as an alternative to the conventional chemical reduction method for the synthesis of nanoparticles (Bastakoti et al., 2015b). This method can control the shape and size of the resulting nanoparticles depending on their encapsulation into mesoporous oxides. For efficient infusion of nanoparticles into the mesopores of metal oxides, the nanocrystal dispersion should flow through the pores by capillary wetting and the nanocrystals must not block the pore openings. In addition, the nanoparticles should exhibit sufficient adsorption to the substrate. Various methods such as supercritical CO_2, ultrasonication, electrophoretic, and direct deposition methods are used to infuse the metal nanoparticles on/into the mesoporous framework (Konya et al., 2003; Xu et al., 2018). Gupta et al. used CO_2 as an antisolvent in toluene to overcome both the transport and thermodynamic challenges encountered during the infusion of nanoparticles into mesoporous silica. They obtained mesoporous silica with nanoparticle loadings of more than 2 wt% in 24 h using carbon dioxide-toluene mixtures (Gupta et al., 2005). Various metal-incorporated mesoporous metal oxides (Pt/SiO_2, Pt/TiO_2, Pt/ZrO_2, Au/TiO_2, and Pd/TiO_2) have been prepared by using a sol-gel process (Liu et al., 2013). Metal nanoparticles exhibit good anti-sintering properties even at high calcination temperatures and metal loadings. Mesoporous oxides are synthesized using mesoporous silica as the hard template. PVP-capped Pt nanoparticles with a size of 2.5 nm can be infused into the mesochannels of such oxides by ultrasonication. Fig. 2 shows the schematic of the synthesis of Pt nanoparticle-incorporated mesoporous oxides and the transmission electron microscopy (TEM) images of the intermediate products obtained during the synthesis process and the final product (An et al., 2013a). Pt nanoparticles strongly adhered to mesoporous metal oxide substrates exhibit excellent CO oxidation performance. In another study, 3-nm Au particles were electrophoretically deposited on a mesoporous TiO_2 film at very high Au nanoparticle loadings (up to 21 %). The nanoparticles were stabilized by dodecanethiol prior to the deposition. The penetration depth of the nanocrystals depended on the strength of the nanoparticles and the wall interactions, which were affected by the dodecanethiol coverage of the metal surface (Patel et al., 2008). Maximum deposition occurs when the pores of the film are perpendicular to the substrate and are aligned with the electric field (Kamada et al., 2004).

The use of the direct film deposition technique for depositing Au nanoparticles on mesoporous silica has been reported. The sol-gel reaction of mesostructure silica was carried out over a monolayer of Au nanoparticles. The shape of the Au nanoparticles could also be changed in-situ through seeded growth and branching. However, the nanoparticles were larger than the silica pores (Angelome et al., 2012). Small nanoparticles can be easily inserted into the mesochannels of porous substrates. Huang et al. synthesized ultrasmall Pt nanoparticles (approximately 1 nm in size) within the branches of polyaminoamide dendrimers. The tertiary amines present in the highly branched dendrimers encapsulated the metal ions and improved the stability of the nanoparticles obtained after the reduction. The silica support immobilized the dendrimer-encapsulated nanoparticles via electrostatic and hydrogen bonding interactions (Huang et al., 2008).

This method yields nanoparticles with desired properties such as optimum stabilizing agent, size, shape, and crystallinity. Prior to the infusion, the particles may be isolated from unwanted byproducts, cleaned, and separated according to their size. Nanoparticles are unstable and should be stabilized using several organic molecules. Some organic molecules play an important role during the chemisorption of particles onto porous substrates. However, particle stabilization using organic molecules is not always necessary. Table 1 summarizes various metal-incorporated porous materials prepared using pre-synthesized metal nanoparticles (Gupta et al., 2006; Fattakhova-Rohlfing et al., 2009; Bore et al., 2006; Ding et al., 2005; Liu et al., 2018; Kim et al., 2015; Chen et al., 2015; Yadav et al., 2019; Zheng and Stucky, 2006; Chen et al., 2012; Chu et al., 2019; Wei et al., 2018).

3.2. Impregnation and reduction

In this method, a metal salt solution is impregnated into a mesoporous substrate followed by reduction of the metal precursors to metallic nanoparticles. The chemical, electrochemical, microwave, plasma, or pulse laser ablation methods are more commonly used for the reduction of metal ions. The metal salt solution either physically adsorbs onto the mesoporous substrate or chemically interacts with it. The isoelectric point (IEP) of the mesoporous substrate and the pH of the solution are very important for creating strong electrostatic interactions between the metal ions and the charged surface of the support. For example, TiO_2 has an IEP of approximately 6. Therefore, at the solution pH values lower than 6, it is positively charged as Ti-OH_2^+. On the other hand, $HAuCl_4$ and H_2PtCl_6 form anionic aqua complexes in water. The strong electrostatic interaction between the anionic metal ions and positively charged substrate surface is the driving force for the adsorption of metal ions on mesoporous materials (Suttiponparnit et al., 2011).

Wen *et al.* synthesized metal nanoparticles encapsulated in the mesochannels of ceria via the impregnation route. First, mesoporous ceria was synthesized by using the hard-templating method. Then, the mesoporous ceria was added to the metal salt solution. The solvent was evaporated, and the dry sample was subsequently reduced by heating. The size of the metal nanoparticles was 3–6 nm. The synthesis mechanism and TEM images of the Au-incorporated mesoporous CeO_2 are shown in Fig. 3 (Wen et al., 2012). Lysine-assisted hydrothermally synthesized mesoporous alumina strongly supports Au nanoparticles with a size of approximately 2 nm. Au nanoparticles are introduced into mesoporous alumina using the deposition and precipitation method followed by annealing in air at elevated temperatures. Annealing is not desirable for Au nanoparticles owing to their low Tammamn temperature (395 °C). However, the strong interfacial interactions between the Au nanoparticles and porous alumina prevent sintering even at high temperatures (up to 900 °C) (Wang et al., 2013). Table 2 summarizes various metal-incorporated nanoporous materials prepared using the impregnation and reduction method (Amin, 2020; Fiorenza et al., 2020; Wang et al., 2015; Chen et al., 2017; Yang et al., 2016; Chen et al., 2008, 2018; Lewis et al., 2019; Lang et al., 2019; Lv et al., 2012; Irandoust and Haghtalab, 2017; Grabchenko et al., 2020).

Campelo et al. reported a quick and environmental friendly method for the preparation of highly active and dispersed mesoporous silica-supported Au and Pd nanoparticles using a microwave technique without using any reducing agent. The microwave irradiation was carried out after soaking the mesoporous silica into the metal salt solution. The rapid heating of the reaction mixtures, especially those containing polar solvents leads to a rapid and almost simultaneous precipitation of the metal solution of the precursor, which in turn

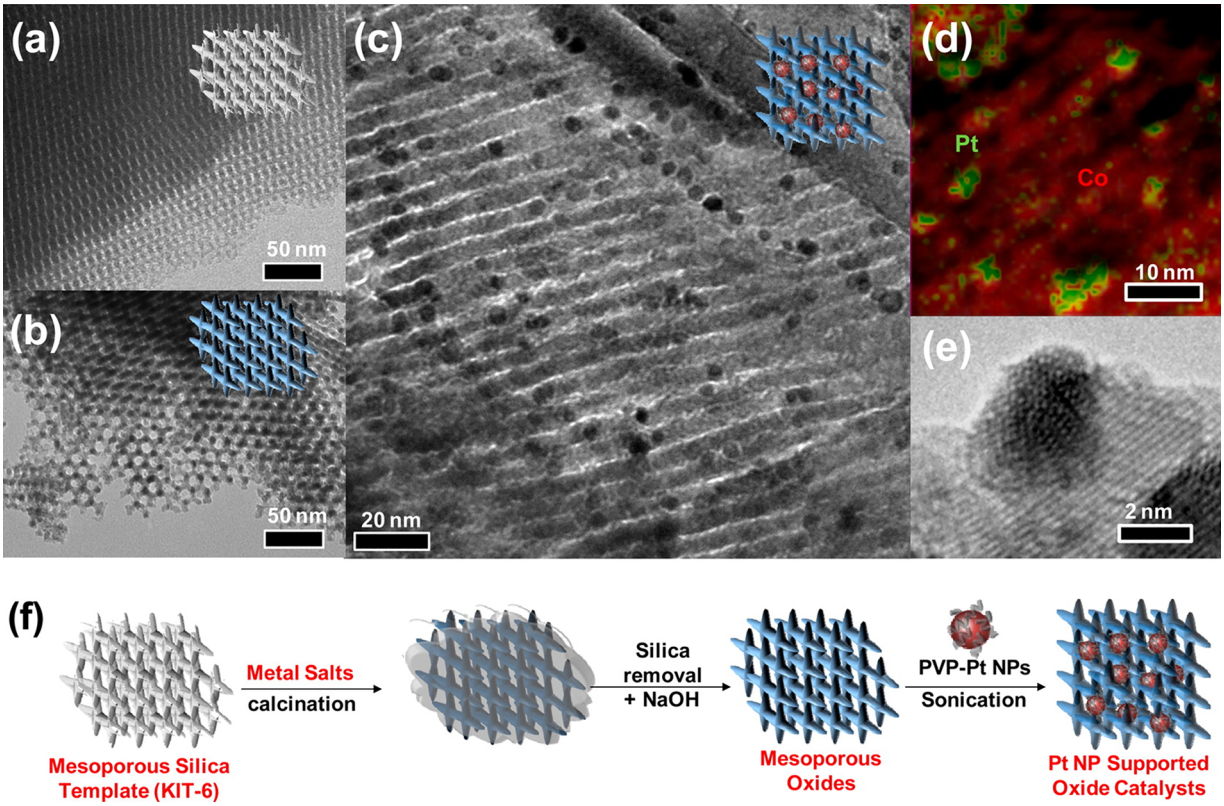

Fig. 2. TEM images of (a) a mesoporous silica template and (b) the resulting Co_3O_4 replica. (c) Pt/Co_3O_4 and (d) their corresponding energy-dispersive spectroscopy image. (e) High-resolution TEM image of Pt/Co_3O_4. (f) Infusing pre-synthesized nanoparticles into mesoporous oxides. Reprinted with permission (An et al., 2013a). Copyright 2013, American Chemical Society.

Table 1
Metal-incorporated porous materials prepared using pre-synthesized metal nanoparticles.

Compositions	Applications	References
Ir@SiO_2	Hydrogenation of decene	(Gupta et al., 2006)
TiO_2@SiO_2	Oxidation of NO	(Fattakhova-Rohlfing et al., 2009)
Au@SiO_2	Oxidation of CO	(Bore et al., 2006)
Pt-Ru@Carbon	Fuel cell reactions	(Ding et al., 2005)
Au@TiO_2	Hydrogenation of methanol	(Liu et al., 2018)
Rh@Carbon	Alcohol synthesis from syngas	(Kim et al., 2015)
Au@zeolite	Oxidation of ethanol	(Chen et al., 2015)
Pt@TiO_2	Hydrogen evolution	(Yadav et al., 2019)
Au@SiO_2	Oxidation of ethanol	(Zheng and Stucky, 2006)
Pd@CeO_2	Oxidation of ethanol	(Chen et al., 2012)
Pt@TiO_2	Computed tomography	(Chu et al., 2019)
Pd,Pt,Au@ZnO, Cu_2O,CeO_2	Hydrogenation of nitroaromics	(Wei et al., 2018)

results in the formation of materials with small particle sizes and narrow size distributions within very short reaction durations (less than 3 min) (Campelo et al., 2008). Highly dispersed metal (Pd, Pt) nanoparticles have been incorporated into SBA-15 via the conventional incipient wetness impregnation method followed by a novel glow discharge plasma reduction. In particular, the plasma reduction at ambient temperature is a green, cost-effective, and rapid reduction method. It offers several advantages over the conventional reduction in the presence of hydrogen at elevated temperatures. Moreover, it requires mild working conditions (Wang et al., 2008a). Instead of wetting the mesoporous substrate by a metal salt solution, Gao and Ying first functionalized SBA-15 with a dendrimer. The Pd^{2+} ions strongly anchored on the dendrimer were reduced to obtain Pd nanoparticles. The very strong anchoring behavior of the dendrimer rendered the resulting Pd nanoparticles highly stable. The Pd nanoparticles could retain their size and activity (Jiang and Gao, 2006). The impregnation and reduction method can be used to load multiple metal nanoparticles on the same mesoporous support.

3.3. One-pot synthesis

This is a relatively easier and faster method for the synthesis of metal-encapsulated mesoporous oxides. In this method, the metal salt, templating agent, and inorganic precursors are mixed together in a single pot avoiding multiple synthesis steps. The metal nanoparticles and mesoporous structure are formed simultaneously. Calcination in an inert medium (N_2 or Ar) during the template removal process reduces the metal precursors to metals and converts the amorphous oxides in the pore walls into crystalline phases (Orilall et al., 2009). Sometimes, H_2 reduction helps to reduce the metal oxides into metals (Wang et al., 2008b).

In general, amphiphilic molecules are used as a template. These molecules co-assemble with the metal and oxide precursors, as shown in Fig. 4a (Orilall et al., 2009). The amphiphilic di-block copolymer poly(isoprene-ethylene oxide) (PI-PEO) acts as a structure-directing agent and provides reaction sites for niobium oxide sols and the metal precursor. The hydrophobic metal precursor is encapsulated into the hydrophobic PI block. Heat treatment in an inert medium removes the PEO unit. The carbonized PI block provides mechanical support to the Nb_2O_5 mesoporous framework and reduces the metal precursors to nanoparticles. Crystalline Nb_2O_5 is obtained by further heating in air (Orilall et al., 2009). A similar amphiphilic diblock copolymer, poly (styrene-ethylene oxide) (PS-PEO) has been used as a template and structure-directing agent for the synthesis of Pt-loaded SiO_2-carbon

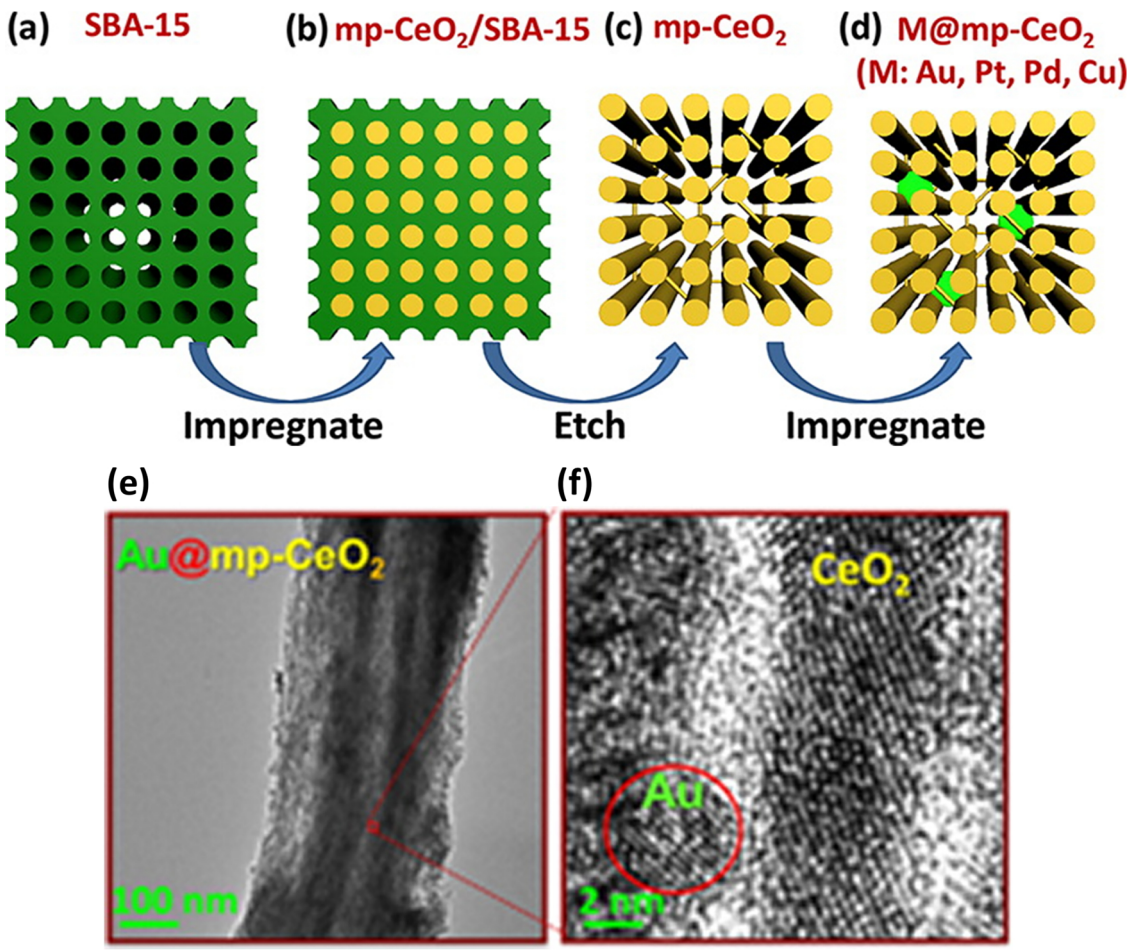

Fig. 3. (a-d) Synthesis of metal nanoparticles in the mesochannels of mesoporous-CeO_2. (e,f) TEM images of metal nanoparticle-encapsulated mesoporous CeO_2. Reprinted with permission (Wen et al., 2012). Copyright 2012, American Chemical Society.

composites. The presence of SiO_2 provides thermal and mechanical stability to the composites. Hydrophilic resols and oligomer silicate species show a large number of −OH groups and can interact strongly with the PEO block, while the hydrophobic metal source selectively interacts with the hydrophobic styrene segments (Shim et al., 2012). Highly dispersed Pd nanoparticles have been encapsulated into MCM-41 using CTA^+ surfactants and Pd^{2+} ions as the capping agents. During the template removal, PdO is formed. This PdO is then reduced to Pd nanoparticles by H_2 reduction. Pd nanoparticles with a particle size of approximately 2 nm have been synthesized in the mesochannels of MCM-41 (Wang et al., 2008b). The in-situ preparation of a mesoporous Pt/TiO_2 nanocomposite using the one-pot synthesis method has been reported. H_2PtCl_6 and titanium butoxides were mixed in the presence of a triblock copolymer, F127, to form ordered micelles. These micelles of F127 acted as a template for the condensation of the inorganic agents. Calcination was carried out in air to remove the polymeric template and render the TiO_2 framework crystalline. The reduction of the Pt source was carried out in a H_2 gas flow at 300 °C (Ismail and Bahnemann, 2011). A multicomponent assembly approach, in which the surfactant, titania and gold precursors are cooperatively assembled in a one-step process, was adopted. Au nanoparticles with a size of 5 nm adhered strongly to the TiO_2 mesochannels. The negative shift in the X-ray photoelectron spectroscopy bands confirmed the existence of a strong interaction between the Au nanoparticles and TiO_2 framework. The

Table 2
Metal-incorporated nanoporous materials prepared using the impregnation and reduction method.

Compositions	Applications	References
$Ni@SiO_2$	CO_2 reforming of Methane	(Amin, 2020)
$Au@CeO_2$	Oxidation of CO	(Fiorenza et al., 2020)
Pt@CN	Oxidation of glycerol	(Wang et al., 2015)
PtFe@Carbon	Hydrogenation of nitrobenzene	(Chen et al., 2017)
M@Carbon(M = Au, Pt, Rh, Ru, Ag, Pd and Ir)	Hydrogenation of benzaldehyde	(Yang et al., 2016)
$Au@M_xO_y$(M = Zr, Ce, Fe, Si)	Oxidation of formaldehyde	(Chen et al., 2008)
$Pt@Cr_2O_3$	Combustion of toluene	(Chen et al., 2018)
AuPdPt@Titanium silicate	Synthesis of H_2O_2	(Lewis et al., 2019)
Pt_1/FeO_x	Combustion of methane	(Lang et al., 2019)
$Ni@SiO_2$	Reforming of methane	(Lv et al., 2012)
$Co\text{-}Ru@Al_2O_3$	Fischer-Tropsch synthesis	(Irandoust and Haghtalab, 2017)
$Ag@CeO_2$	Oxidation of CO	(Grabchenko et al., 2020)

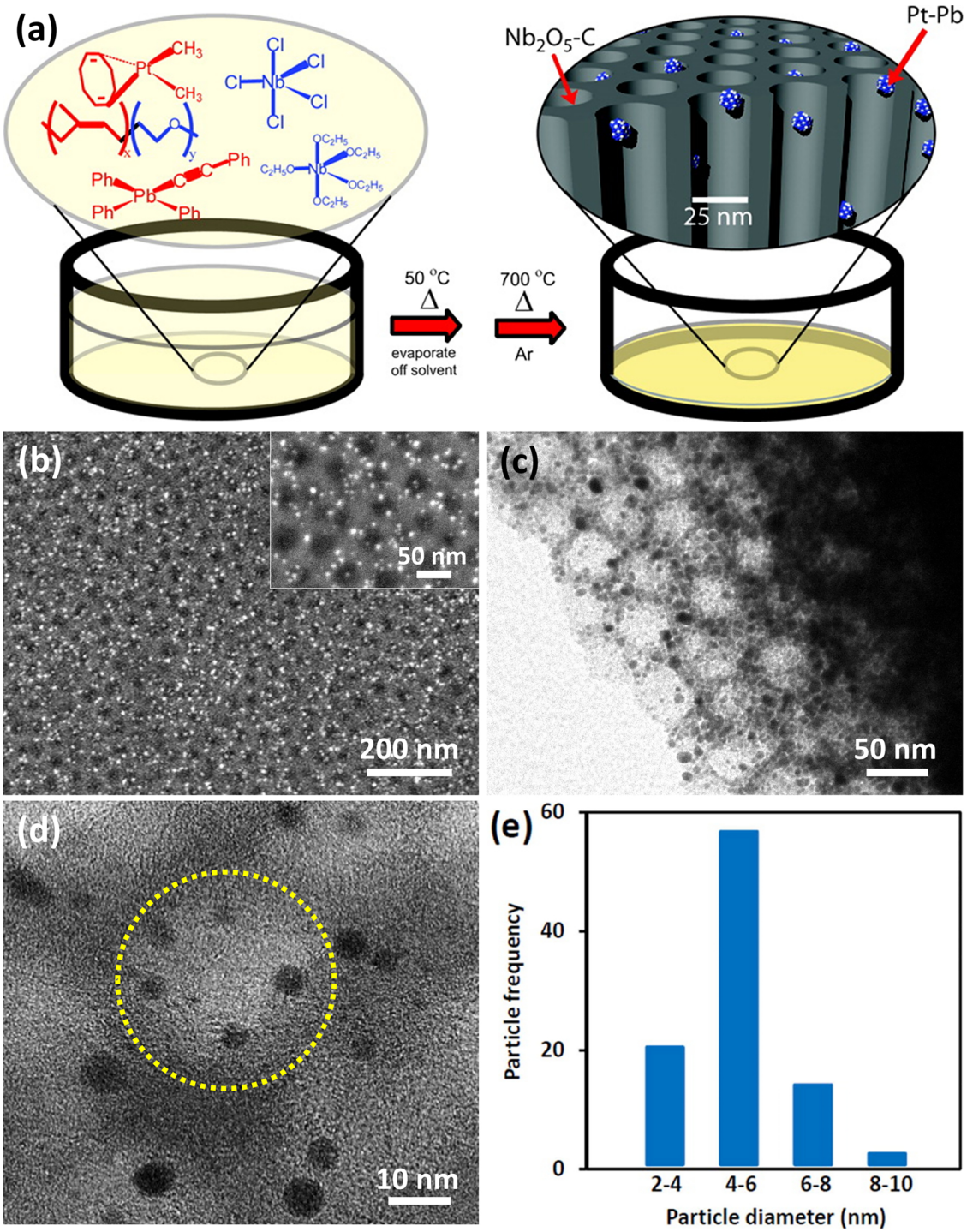

Fig. 4. (a) Illustration of the one-pot synthesis of metal-incorporated mesoporous supports. Reprinted with permission. (Orilall et al., 2009) Copyright 2009, American Chemical Society. (b) scanning electron microscopy and (c and d) TEM images of Pt-incorporated mesoporous SiO_2. (e) Particle-size distribution of Pt nanoparticles. Reprinted with permission (Bastakoti et al., 2014a). Copyright 2014, Royal Chemical Society.

nanoparticle dimensions depended on the Au precursor amount (Li et al., 2007a). Morris et al. developed a method to synthesize alumina-supported structures via the simultaneous self-assembly of aluminum isopropoxide, the metal precursors, and the P123 triblock copolymer. Compared to pure alumina, nickel aluminum oxides show improved thermal stability. Very high metal loadings, large and accessible pores, and the generality of the synthetic route represent the important steps towards the facile one-pot synthesis of alumina-supported materials (Morris et al., 2008).

We reported the synthesis of Pt-incorporated mesoporous metal oxides via the self-assembly of polymeric micelles of asymmetric triblock copolymers. The micelles of poly(styrene-2-vinylpyridine-ethylene oxide) (PS-PVP-PEO) facilitated the direct synthesis of Pt-decorated mesoporous TiO_2, Al_2O_3, and SiO_2 (Fig. 4b-e) (Bastakoti et al., 2014a). The hydrophobic interaction of platinum- (II) 2,4-pentanedionate with the PS block and the electrostatic interaction between the oxide precursors and the PVP block enabled the successful incorporation of Pt nanoparticles into the pores of the mesoporous oxides (Bastakoti et al., 2014b). As PVP blocks can arrest a wide range of metal sources, the composition of such mesoporous frameworks can be easily

Table 3
Metal-incorporated nanoporous materials prepared using the one-pot synthesis method.

Compositions	Applications	References
$Ni@Al_2O_3$	–	(Morris et al., 2008)
Pt-Pb@NbO_2-carbon	Fuel cells	(Orilall et al., 2009)
Pd@$CoFe_2O_4$-graphene	Reduction of nitrophenol	(Lu et al., 2014)
Pt@CeO_{2-x} /graphene	Oxidation of alcohol	(Zhang and Shen, 2015)
$Cu@SiO_2$	Dehydrogenation of borane	(Yao et al., 2014)
Au@M_xO_y (M = Co, Ce, Fe, and Sn)	Oxidation of CO	(Li et al., 2018a)
$Ni@SiO_2$	Dry reforming of methane	(Wang et al., 2017a)
Au, Ag@polyaniline	–	(Pillalamarri et al., 2005)
$Au@SiO_2$	Hydroamination of alkyne	(Solovyeva et al., 2014)
Ni-Mo@Al_2O_3	Hydrodesulfurization	(Yi et al., 2017)
$Ag@SiO_2$	Antibacterial activity	(Tian et al., 2014)
Pt, Pd@ZnO	Reduction of nitrophenol	(Bao et al., 2017)

controlled (Bastakoti et al., 2014c). The shell thickness and pore diameter can be easily tuned by changing the molecular weight of the block copolymer or the precursor/polymer ratio. The facile '*polymeric micelle assembly*' approach is beneficial for the deposition of fully accessible and uniformly dispersed metal nanoparticles on/into the mesopores of the substrate. Table 3 summarizes various metal-incorporated nanoporous materials prepared using the one-pot synthesis method (Morris et al., 2008; Orilall et al., 2009; Lu et al., 2014; Zhang and Shen, 2015; Yao et al., 2014; Li et al., 2018a; Wang et al., 2017a; Pillalamarri et al., 2005; Solovyeva et al., 2014; Yi et al., 2017; Tian et al., 2014; Bao et al., 2017).

In spite of its simplicity, the one-pot synthesis method shows several disadvantages. Selecting appropriate concentrations of different ingredients is very important for the synthesis of a well-organized cooperative assembly. Metal precursors interfere with the polymerization reaction of the alkoxide precursors. The competition between the metal and metal oxide precursors and the template, heterogeneous nature of hydrolysis, and condensation of metal oxides make the one-pot synthesis of metal-loaded mesoporous metal oxides challenging. This method offers less control over the size of nanoparticles because of the presence of various interfering agents such as counter ions and the simultaneous interaction of the metal salt and inorganic oligomers with the organic template. However, if a reduction step is used after the one-pot reaction, the size of the resulting nanoparticles can be easily controlled. Liu et al. used a steaming reduction process to control the size of nanoparticles synthesized via the one-pot method. With an increase in the reduction time from 1 to 24 h, the particle size increased from 1.4 to 4.5 nm (Liu et al., 2014).

Gonçalves and Jaroniec controlled the solvent exchange to tune the hydrolysis and condensation rate of oxide precursors to stabilize the mesophase formation (Fig. 5) (Goncalves and Jaroniec, 2019). The difference in the solubility, hydrolysis, and condensation of the Ni, Al, and Zr precursors in different solvents affected the mesophase formation in the Ni-Al-Zr ternary oxides. The oxides synthesized in the presence of isopropanol and n-propanol showed similar textural properties. The slightly higher specific surface area and pore volume of the oxide synthesized in the presence of propanol (Fig. 5b) can be attributed to the poor solubility of zirconium n-propoxide in propanol. The use of ethanol as the solvent rendered the mesophase unstable. This is because both the aluminum and zirconium precursors showed high reactivity towards ethanol. These results demonstrate the importance of rationalizing the entropic changes during the synthesis of nanostructured solids by the evaporation-induced self-assembly process (Goncalves and Jaroniec, 2019; Goncalves et al., 2018).

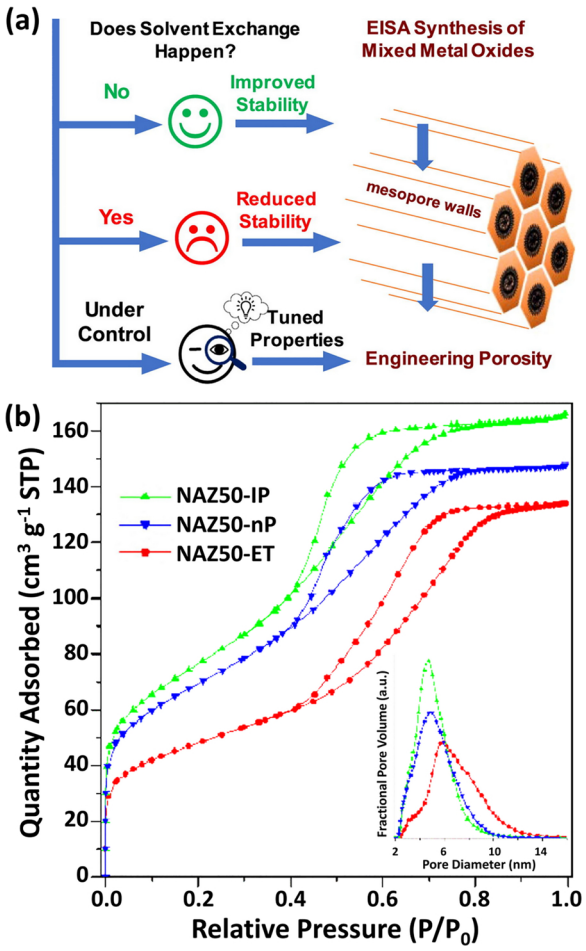

Fig. 5. (a) Solvent exchange to control the mesostructure. (b) Nitrogen sorption isotherms for nanostructured Ni-Al-Zr ternary mixed oxides synthesized in ethanol (NAZ50-ET), isopropanol (NAZ50-IP), and n-propanol (NAZ50-nP) and their pore size distribution curves. Reprinted with permission (Goncalves and Jaroniec, 2019). Copyright 2018, Elsevier Inc.

4. Applications

4.1. Novel catalysts for environmental remediation

Metal-supported catalysts are widely used in various catalytic reactions (Morris et al., 2008; Xu et al., 2020; Cai et al., 2011). Among these reactions, the catalytic oxidation of CO has been widely investigated as a typical model reaction. CO is a toxic gas, which is produced by the incomplete combustion of carbon-containing fuels. CO oxidation is practically important for the purification of engine exhaust gases. Pt, Pd, and Au nanoparticles show high catalytic activities towards the oxidation of CO, and mesoporous TiO_2, CeO_2, SiO_2 are the most promising supports. Haruta prepared several supported metal catalysts and compared their activities for CO oxidation. He found that the CO oxidation activities of the metal catalysts followed the order: Au > Pd > Rh > Pt > Ir > Ru > Ag. The optimum particle size for the Au catalyst was found to be approximately 3 nm. The efficacy of the supports for the oxidation reaction followed the order: CeO_2 > ZrO_2 > Al_2O_3 > SiO_2 (Haruta, 2003). Somorjai et al. prepared several Pt-based catalysts for the oxidation of CO. The turnover frequencies of the Pt-loaded mesoporous supports were significantly higher than those calculated by simply summing the contributions from each of the constituents. This can be attributed to the synergic effect of the oxide and metal. The in-situ studies revealed that the redox reactions of the oxides generated charged species, which altered the CO oxidation mechanism.

The CO oxidation rates of the Pt-nanoparticle-loaded oxide catalysts were affected by the redox properties of the oxides at the oxide-metal interface under reducing reaction conditions. The Pt/Co_3O_4 catalyst showed the highest catalytic turnover among all the catalysts investigated (). This is probably because of the efficient charge transfer due to the higher concentration of electrons in the interfacial region of this catalyst.

As a fuel, H_2 is a promising alternative to fossil fuels as it produces only H_2O during combustion. Metal oxide-supported catalysts have been used for the steam reforming of alcohols to produce H_2 for automobiles and fuel cell applications. In supported metal catalysts, both the metal and the mesoporous support play a significant role in improving the selectivity for H_2 production. In a study on the steam reforming of methanol (SRM), Cu exhibited better methanol conversion and higher hydrogen selectivity than all the other metals investigated when mesoporous silica such as MCM-41 was used as the support (Abrokwah et al., 2016). Significant difference was observed in the methanol conversion and hydrogen selectivity of the catalysts when the MCM-41 support was replaced with a mesoporous TiO_2 support (Deshmane et al., 2015). Zn/TiO_2 showed better SRM catalytic activity than the other catalysts investigated. To increase the stability of the catalyst and suppress the formation of CO, CeO_2, TiO_2, and MgO were added to the MCM-41- or SBA-15-supported Ni or Co-catalysts. The 10 %Ni-MCM-41 catalyst with 5 % CeO_2 or TiO_2 exhibited excellent catalytic stability for glycerol steam reforming over 40 h. Addition of 5 % MgO to Ni-SBA-15 or Co-SBA-15 significantly improved the long-term stability of both the catalysts (Bepari and Kuila, 2020; AlSalihi et al., 2020). In another study, Ni-incorporated Al_2O_3 and Al_2O_3-TiO_2 supports were used for the steam reforming of ethanol to produce H_2 (Fig. 6a, b) (Goncalves et al., 2017). TiO_2 played a vital role in tailoring the acidic and basic properties of the composites. The acidic sites of the Ni-Al oxide composites decreased with the addition of TiO_2, which in turn weakened the interaction of ethanol and the byproducts with the Al_2O_3-TiO_2 support, thus retarding the accumulation of coke during the reaction (Goncalves et al., 2017).

Kuila *et al.* used metal-loaded mesoporous supports for the conversion of syngas (CO and H_2) into hydrocarbons. In a previous study, a uniform coating of the sol-gel catalyst layer in the microchannels of Si-microreactors produced C_1-C_4 alkanes at 1 atm (Zhao et al., 2008). The support showed a significant effect on the CO conversion and stability of the catalyst. On the other hand, the Co-catalyst showed higher CO conversion and stability than Fe and Ru in the SiO_2 sol-gel (Abrokwah et al., 2019). Unlike the case with the SiO_2-supported catalysts, Ru-TiO_2 showed much higher stability than the Co- and Fe-TiO_2 catalysts in Fisher-Tropsch (F–T) synthesis. The rutile phase of TiO_2 played a significant role in catalyzing the F–T synthesis. In order to investigate the effect of the 2nd metal on the F–T synthesis, Mohammed et al. (Mohammad et al., 2020) added Fe, Ru, and Ni to Co-MCM-41 with large surface area and carried out CO conversion in a three-dimensional (3D) printed microreactor. The addition of the 2nd metal increased the CO conversion efficiency of Co-MCM-41 by 65–78 %. The reaction temperature also affected CO conversion of the catalyst. The presence of Ni did not favor the formation of propane and butane, while both Ru and Fe showed a positive effect. Over the temperature range of 270–300 °C, the CoFe bimetallic catalyst showed the propane and butane selectivities of 39 and 8 %, respectively. On the other hand, the CoRu

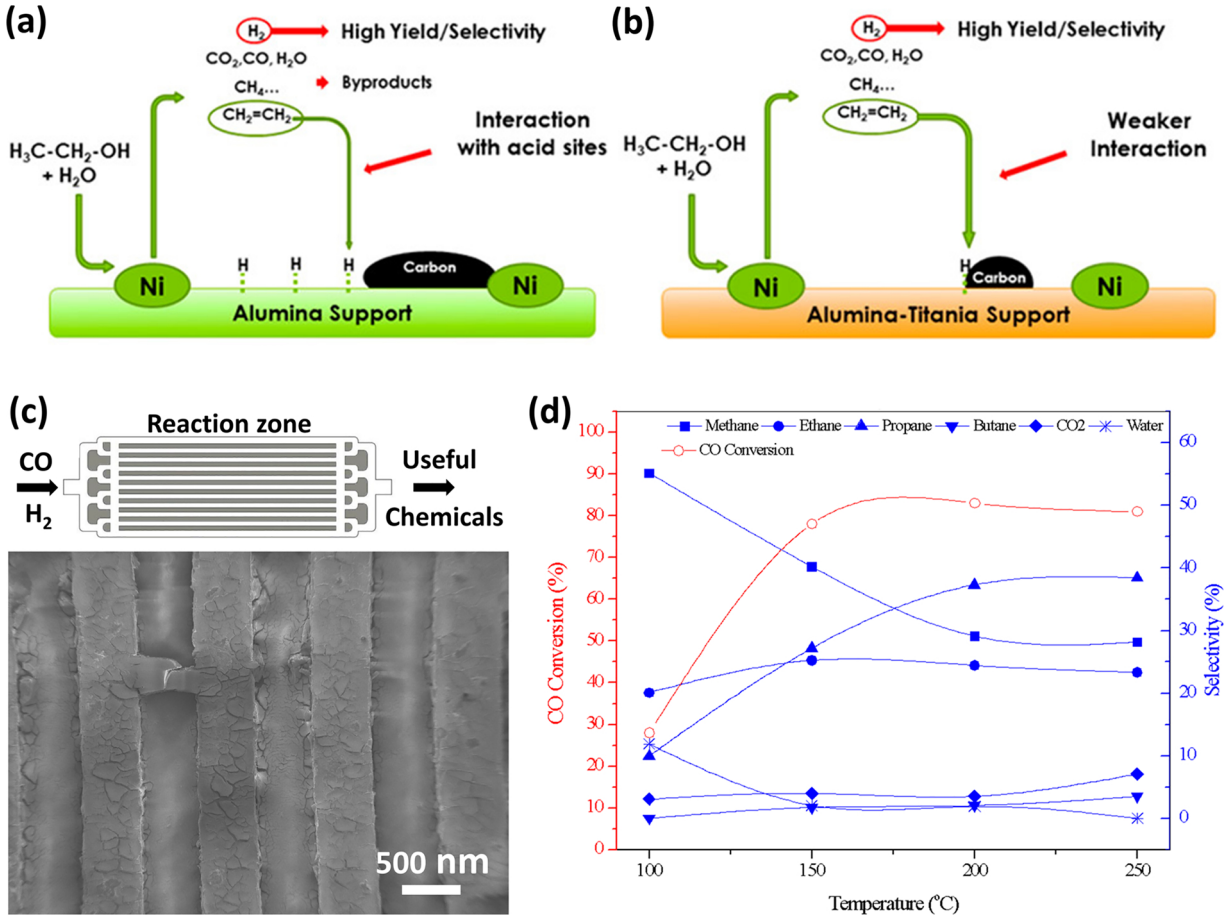

Fig. 6. Steam reforming of ethanol over (a) Ni-Al_2O_3 and (b) Ni-Al_2O_3-TiO_2 catalysts. Reprinted with permission (Goncalves et al., 2017). Copyright 2017, American Chemical Society. (c) Fischer-Tropsch synthesis: 3D printed micro-reactor design and metal-decorated oxide catalyst-coated microchannels. (d) CO selectivity and conversion (into hydrocarbons) in Si-microchannel microreactors. Reprinted with permission (Mohammad et al., 2019). Copyright 2019, Molecular Diversity Preservation International.

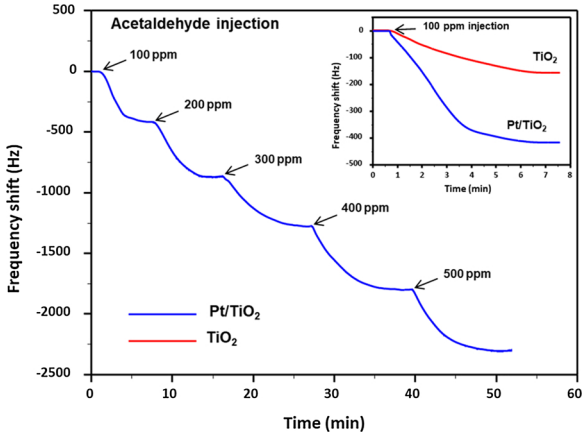

Fig. 7. Time-dependent frequency shift curve of QCM coated with pure mesoporous TiO_2 (red line) and Pt-decorated mesoporous TiO_2-based films (blue line) caused by exposure to different concentrations of vaporized acetaldehyde. Reprinted with permission (Bastakoti et al., 2014b). Copyright 2014, American Chemical Society.

catalyst showed higher propane and butane selectivities of 33.5 and 11.2 %, respectively at 210 °C (Mohammad et al., 2019). In addition, the FeCo catalyst showed much higher stability than the other bimetallic catalysts. To investigate the effects of the metal-support interactions, catalyst morphology, and mesoporous SiO_2-structure on the kinetics of the F–T reaction, Co and Ru bimetallic nanocatalysts were loaded into MCM-41, SBA-15, and KIT-6 using a one-pot procedure. The catalysts were coated in 3D printed stainless steel microchannels using a slurry method (Fig. 6c, d). Mesoporous silica supports significantly affect the F–T kinetics and stability of metal catalysts. The activation energy calculations revealed that the activity of CoRu-KIT-6 was 2.5 times higher than that of Co-Ru-MCM-41 and slightly higher than that of CoRu-SBA-15. The CO conversion capacities of the catalysts measured during the deactivation studies indicated that CoRu-KIT-6 was ~3 and ~1.5 times more stable than CoRu-SBA-15 and CoRu-MCM-41, respectively (Mohammad et al., 2019).

Supported metal catalysts are also used for degrading organic molecules (pollutants). The mesoporous support not only increases the reactivity but also facilitates the recycling of the catalyst (Lu et al., 2013; Ahmed et al., 2017; Li et al., 2007b). Furthermore, the introduction of nanoparticles into a mesoporous support decreases the gap between the intraband state and the conduction band or valence band edge by forming a sub-band gap. This sub-band gap serves as an electronic trap by providing defective sites. The use of porous supports also significantly increases the adsorption capacity of the catalyst. Organic molecules move to the metal surface to enhance the degradation rate (Li et al., 2007a). Ag-loaded mesoporous WO_3 shows excellent activity for the degradation of acetaldehyde in the presence of visible light. The excellent photocatalytic activity of this catalyst can be attributed to the electron-hole separation at the Ag-WO_3 heterojunction (Sun et al., 2010). The photoinduced holes react with H_2O or OH^- to produce the hydroxyl radical (·OH), which is an extremely strong oxidant for the degradation of organic contaminants (Hayyan et al., 2016). When Ag nanoparticles come in contact with WO_3, the electrons migrate from Ag to the conduction band of WO_3 to achieve the Fermi level equilibrium. As a result, the surface of the WO_3 accumulates excess electrons, while Ag exhibits excess positive charge. Thus, a deflexed energy band is formed at the Ag-WO_3 interface, which generates more holes in the valence band of WO_3. In another study, Gao et al. used Pd-In nanoparticle-loaded mesoporous Al_2O_3 to reduce nitrate ions into N_2 and NH_3 (Gao et al., 2015). The overuse of nitrogen-rich fertilizers in agriculture has contaminated the ground water with nitrate ions. The catalytic reduction of nitrate ions is a promising technology for groundwater purification because it transforms nitrate ions into nitrogen, ammonia, and water.

4.2. Catalysts for sensing hazardous materials

Sensing hazardous materials is a key technology that finds applications in many technical processes, environmental monitoring, and automobiles (Wang et al., 2017b; Bahadur et al., 2011; Koo et al., 2016; Tomer et al., 2014). Transition metal oxides, such as TiO_2, SnO_2, WO_3, Cr_2O_3, and In_2O_3, are widely used for developing semiconductor sensors (Meixner et al., 1995; Mccue and Ying, 2007; Choi et al., 2014; Wang et al., 2006). The sensitivity of these oxides towards hazardous materials depends on their morphology and conductivity. Metal nanoparticles such as Pt and Pd show excellent chemical and electronic sensitization (Yamazoe et al., 1983). Ag nanoparticle-loaded mesoporous Cr_2O_3 microspheres show excellent triethylamine detection. Ag nanoparticles improve the triethylamine selectivity of mesoporous Cr_2O_3 microspheres at low working temperatures (Cao et al., 2015). Recently, we developed Pt-decorated mesoporous TiO_2 for sensing various volatile organic solvents using a quartz crystal microbalance (QCM)-based technique(Bastakoti et al., 2014b). The QCM-based sensing method enables the real-time monitoring of the sorption of vapor molecules. The frequency of a quartz electrode changes when a small amount (nanogram scale) of vapor is adsorbed onto its surface. The sensing efficiency of a material can be determined by measuring its frequency. The dynamic response of the Pt-decorated mesoporous TiO_2 electrode upon exposure to acetaldehyde vapor with different concentrations ranging from 100 to 500 ppm is shown in Fig. 7 (Bastakoti et al., 2014b). Compared to the mesoporous TiO_2 sensor, the Pt-decorated mesoporous TiO_2-based sensor showed almost 2.5 times higher acetaldehyde vapor uptake. This can be attributed to the presence of metallic Pt, which remarkably enhanced the sensing property of mesoporous TiO_2 through the chemical sensitization mechanism. The Pt nanoparticles not only provided abundant adsorption sites for the incoming gas molecules but also facilitated the spillover of oxygen species onto the TiO_2 surface, where they ionosorbed by trapping electrons from TiO_2 (dipole-dipole interaction with the oxygen surface of TiO_2) (Bastakoti et al., 2014b). Li et al. systematically investigated the NO_2sensing ability of Au-loaded mesoporous In_2O_3. The 0.5 wt% Au-loaded In_2O_3 catalyst exhibited excellent sensor response with a low detection limit of 10 ppb at a low operating temperature of 65 °C (Li et al., 2018b). Zalduendo et al. used nanocomposites of Au nanoparticles and mesoporous TiO_2 as surface-enhanced Raman scattering sensors. The dendritic Au nanoparticles covered with mesoporous TiO_2 showed a detection limit as low as 10 pM (Zalduendo et al., 2018).

Defects in either the metal catalyst or support significantly affect the sensing performance of metal oxide-supported metal catalysts (Shen et al., 2020; Zhang et al., 2020b; Sterrer et al., 2006; Dey, 2018; Zhang et al., 2019b). These defects introduce new acceptor or donor levels and provide sufficient mobility of electrons. Oxygen vacancies in the support act as adsorption sites and nucleation centers for metal clusters/nanoparticles (Dey, 2018). Al doping generates oxygen vacancies in TiO_2 and increases its conductivity. Al-doped TiO_2 sensors are more sensitive and selective to oxygen and carbon monoxide than pure TiO_2 sensors (Choi et al., 2007). The addition of Au nanoparticles on the basal plane of nitrogen-doped graphene quantum dots (N-GQDs) reduces the number of defects by decreasing the N and O % in Au@NGQD composites. This enhances the charge carrier mobility of N-GQDs and produces an ultrafast photoresponse (Das et al., 2020). Zhang et al. used bimetallic nanoparticles of Au and Pt for the selective detection of dopamine. Different metals grow independently and show random growth orientations. This generates multiple surface defects such as twin boundaries, dislocations, stacking faults, and interstitial defects on bimetallic nanoparticles (Zhang et al., 2020b).

5. Conclusion and future perspective

In this review, we have summarized the recent developments in the synthesis and applications of metal-incorporated mesoporous metal

oxides. Owing to their ultrasmall size, nanoparticles are very reactive and tend to aggregate. The anchoring of metal nanoparticles on/into mesoporous frameworks not only stabilizes the nanoparticles but also induces a synergistic effect, which is exploited in a wide range of applications. The lattice mismatch between the metal nanoparticles and metal oxide surface provides extra stability to metal-incorporated mesoporous metal oxides. The adhesion energies between the metal nanoparticles and metal oxide surface create a repulsive interaction between the neighboring metal nanoparticles. These repulsive interactions act as an activation barrier to prevent the agglomeration of the nanoparticles. The recent advances in the design and synthesis of metal-incorporated mesoporous metal oxides have led to the synthesis of various novel materials suitable for various applications. The advantage of using pre-synthesized nanoparticles for the preparation of metal-incorporated mesoporous metal oxides is that the desired nanoparticle properties such as the size, shape, and crystallinity can be achieved prior to the nanoparticle infusion into the support. The one-pot synthesis method is relatively easier and faster than the other methods used for the preparation of metal-incorporated mesoporous metal oxides as it avoids multiple synthesis steps. Controlling the solvent exchange during the condensation and hydrolysis reaction of metal oxides stabilizes the mesophase formation. The impregnation and reduction methods are useful to control the nanoparticle size and to load multiple metal nanoparticles on the same mesoporous support. These metal-incorporated mesoporous metal oxide materials have been widely investigated for various applications such as sensing hazardous chemicals and the conversion of pollutants into useful chemicals. However, most of the studies on support materials are limited to a few metal oxides such as SiO_2, Al_2O_3, TiO_2, Co_3O_4, and CeO_2. Thus, there is a limited scope to tailor the properties of metal-incorporated mesoporous metal oxides. In the future, more attention should be paid on the design of novel metal-support combinations with improved catalytic performance.

CRediT authorship contribution statement

Bishnu Prasad Bastakoti: Conceptualization, Investigation, Methodology, Resources, Validation, Visualization, Writing - original draft, Writing - review & editing, Project administration, Funding acquisition. **Debasish Kuila:** Investigation, Methodology, Resources, Validation, Visualization, Writing - original draft, Writing - review & editing, Funding acquisition. **Carlos Salomon:** Writing - review & editing. **Muxina Konarova:** Writing - review & editing. **Miharu Eguchi:** Writing - review & editing. **Jongbeom Na:** Investigation, Methodology, Resources, Validation, Visualization, Writing - original draft, Writing - review & editing. **Yusuke Yamauchi:** Conceptualization, Investigation, Methodology, Resources, Validation, Visualization, Writing - original draft, Writing - review & editing.

Declaration of Competing Interest

The authors declare that they have no known competing financial interests or personal relationships that could have appeared to influence the work reported in this paper.

Acknowledgement

This work is supported by the National Science Foundation (NSF) Research Initiation Awad, USA (2000310), NSF CREST, USA (260326), the University of North Carolina, Research Opportunity Initiative, USA (110092), the Australian Research Council (ARC) Discovery Project, Australia (DP190102944), and Future Fellow, Australia (FT150100479). This work is partially performed at the Queensland node of the Australian National Fabrication Facility, a company established under the National Collaborative Research Infrastructure Strategy to provide nano- and micro-fabrication facilities for Australian researchers. The authors also acknowledge the facilities, and the scientific and technical assistance, of the Australian Microscopy & Microanalysis Research Facility at the Centre for Microscopy and Microanalysis, The University of Queensland.

References

Abrokwah, R.Y., Deshmane, V.G., Kuila, D., 2016. Comparative performance of M-MCM-41 (M: Cu, Co, Ni, Pd, Zn and Sn) catalysts for steam reforming of methanol. J. Mol. Catal. A-Chem. 425, 10–20.

Abrokwah, R.Y., Rahman, M.M., Deshmane, V.G., Kuila, D., 2019. Effect of titania support on Fischer-Tropsch synthesis using cobalt, iron, and ruthenium catalysts in silicon-microchannel microreactor. Mol. Catal. 478, 110566.

Ahmed, M.A., Messih, M.F.A., El-Sherbeny, E.F., El-Hafez, S.F., Khalifa, A.M.M., 2017. Synthesis of metallic silver nanoparticles decorated mesoporous SnO_2 for removal of methylene blue dye by coupling adsorption and photocatalytic processes. J. Photochem. Photobiol. A: Chem. 346, 77–88.

AlSalihi, W.D.S., Swain, J., Abrokwah, R., Deshmane, V., Hossain, T., Kuila, D., 2020. Mesoporous MCM-41 and SBA-15 supported Co and Ni catalysts for steam reforming of Glycerol to produce hydrogen. Int. J. Hydrogen Energy In press.

Amin, M.H., 2020. Relationship between the pore structure of mesoporous silica supports and the activity of nickel nanocatalysts in the CO2 reforming of methane. Catalysts 10, 51.

An, K., Alayoglu, S., Musselwhite, N., Plamthottam, S., Melaet, G., Lindeman, A.E., Somorjai, G.A., 2013a. Enhanced CO oxidation rates at the interface of mesoporous oxides and Pt nanoparticles. J. Am. Chem. Soc. 135, 16689–16696.

Angelome, P.C., Pastoriza-Santos, I., Perez-Juste, J., Rodriguez-Gonzalez, B., Zelcer, A., Soler-Illia, G.J., Liz-Marzan, L.M., 2012. Growth and branching of gold nanoparticles through mesoporous silica thin films. Nanoscale 4, 931–939.

Au, C.-T., Liao, M.-S., Ng, C.-F., 1998. A detailed theoretical treatment of the partial oxidation of methane to syngas on transition and coinage metal (M) catalysts (M = Ni, Pd, Pt, Cu). J. Phys. Chem. A 102, 3959–3969.

Bahadur, N., Jain, K., Pasricha, R., Govind, Chand, S., 2011. Selective gas sensing response from different loading of Ag in sol-gel mesoporous titania powders. Sens. Actuators B-Chem. 159, 112–120.

Bao, Z., Yuan, Y., Leng, C., Li, L., Zhao, K., Sun, Z., 2017. One-pot synthesis of noble Metal/Zinc oxide composites with controllable morphology and high catalytic performance. ACS Appl. Mater. Interfaces 9, 16417–16425.

Barcaro, G., Fortunelli, A., 2019. 2D oxides on metal materials: concepts, status, and perspectives. Phys. Chem. Chem. Phys. 21, 11510–11536.

Barman, S.R., Nain, A., Jain, S., Punjabi, N., Mukherji, S., Satija, J., 2018. Dendrimer as a multifunctional capping agent for metal nanoparticles for use in bioimaging, drug delivery and sensor applications. J. Mater. Chem. B 2368–2384.

Bastakoti, B.P., Guragain, S., Yokoyama, Y., Yusa, S., Nakashima, K., 2011. Synthesis of hollow $CaCO_3$ nanospheres templated by Micelles of poly(styrene-b-acrylic acid-b-ethylene glycol) in aqueous solutions. Langmuir 27, 379–384.

Bastakoti, B.P., Guragain, S., Yusa, S., Nakashima, K., 2012. Novel synthesis route for $Ag@SiO_2$ core-shell nanoparticles via micelle template of double hydrophilic block copolymer. RSC Adv. 2, 5938–5940.

Bastakoti, B.P., Li, Y., Miyamoto, N., Sanchez-Ballester, N.M., Abe, H., Ye, J., Srinivasu, P., Yamauchi, Y., 2014a. Polymeric micelle assembly for the direct synthesis of functionalized mesoporous silica with fully accessible Pt nanoparticles toward an improved CO oxidation reaction. Chem. Commun. 50, 9101–9104.

Bastakoti, B.P., Torad, N.L., Yamauchi, Y., 2014b. Polymeric micelle assembly for the direct synthesis of platinum-decorated mesoporous TiO_2 toward highly selective sensing of acetaldehyde. ACS Appl. Mater. Interfaces 6, 854–8560.

Bastakoti, B.P., Ishihara, S., Leo, S.-Y., Ariga, K., Wu, K.C.-W., Yamauchi, Y., 2014c. Polymeric micelle assembly for preparation of large-sized mesoporous metal oxides with various compositions. Langmuir 30, 651–659.

Bastakoti, B.P., Li, Y., Kimura, T., Yamauchi, Y., 2015a. Asymmetric block copolymers for supramolecular templating of inorganic nanospace materials. Small 11, 1992–2002.

Bastakoti, B.P., Sakka, Y., Wu, K.C.W., Yamauchi, Y., 2015b. Synthesis of highly photocatalytic TiO_2 microflowers based on solvothermal approach using N-Dimethylformamide. J. Nanosci. Nanotechnol. 15, 4747–4751.

Bastús, N.G., Merkoçi, F., Piella, J., Puntes, V., 2014. Synthesis of highly monodisperse citrate-stabilized silver nanoparticles of up to 200 nm: kinetic control and catalytic properties. Chem. Mater. 26, 2836–2846.

Bepari, S., Kuila, D., 2020. Steam reforming of methanol, ethanol and glycerol over nickel-based catalysts-A review. Int. J. Hydrogen Energy In press.

Bond, G.C., Thompson, D.T., 1999. Catalysis by gold. Catal. Rev. 4, 319–388.

Bore, M.T., Mokhonoana, M.P., Ward, T.L., Coville, N.J., Datye, A.K., 2006. Synthesis and reactivity of gold nanoparticles supported on transition metal doped mesoporous silica. Microporous Mesoporous Mater. 95, 118–125.

Cai, W.Q., Yu, J.G., Cheng, B., Su, B.L., Jaroniec, M., 2009. Synthesis of boehmite hollow core/shell and hollow microspheres via sodium tartrate-mediated phase transformation and their enhanced adsorption performance in water treatment. J. Phys. Chem. C 113, 14739–14746.

Cai, W., Yu, J., Anand, C., Vinu, A., Jaroniec, M., 2011. Facile synthesis of ordered mesoporous alumina and alumina-supported metal oxides with tailored adsorption and framework properties. Chem. Mater. 23, 1147–1157.

Caldas, P.C.P., Gallo, J.M.R., Lopez-Castillo, A., Zanchet, D., Bueno, J.M.C., 2017. The structure of the Cu-CuO sites determines the catalytic activity of Cu nanoparticles.

ACS Catal. 7, 2419–2424.
Campbell, C.T., Parker, S.C., Starr, D.E., 2002. The effect of size-dependent nanoparticle energetics on catalyst sintering. Science 298, 811–814.
Campelo, J.M., Conesa, T.D., Gracia, M.J., Jurado, M.J., Luque, R., Marinas, J.M., Romero, A.A., 2008. Microwave facile preparation of highly active and dispersed SBA-12 supported metal nanoparticles. Green Chem. 10, 853–858.
Cao, J., Xu, Y., Sui, L., Zhang, X., Gao, S., Chen, X.L., Zhao, H., Huo, L., 2015. Highly selective low-temperature triethylamine sensor based on Ag/Cr_2O_3 mesoporous microspheres. Sens. Actuators B-Chem. 220, 910–918.
Cargnello, M., Doan-Nguyen, V.V.T., Gordon, T.R., Diaz, R.E., Stach, E.A., Gorte, R.J., Fornasiero, P., Murray, C.B., 2013. Control of metal nanocrystal size reveals metal-support interface role for Ceria catalysts. Science 341, 771–773.
Chaudhuri, R.G., Paria, S., 2012. Core/shell nanoparticles: classes, properties, synthesis mechanisms, characterization, and applications. Chem. Rev. 112, 2373–2433.
Chen, X., Zhu, H.-Y., Zhao, J.-C., Zheng, Z.-F., Gao, X.P., 2008. Visible-light-driven oxidation of organic contaminants in air with gold nanoparticle catalysts on oxide supports. Angew. Chemie Int. Ed. English 47, 5353–5356.
Chen, C., Fang, X., Wu, B., Huang, L., Zheng, N., 2012. A multi-yolk-Shell structured nanocatalyst containing Sub-10 nm Pd nanoparticles in porous CeO_2. ChemCatChem 4, 1578–1586.
Chen, H., Jia, X., Li, Y., Liu, C., Yang, Y., 2015. Controlled surface properties of Au/ZSM5 catalysts and their effects in the selective oxidation of ethanol. Catal. Today 256, 153–160.
Chen, H., He, D., He, Q., Jiang, P., Zhou, G., Fu, W., 2017. Selective hydrogenation of p-chloronitrobenzene over an Fe promoted Pt/AC catalyst. RSC Adv. 7, 29143–29148.
Chen, X., Chen, X., Cai, S., Chen, J., Xu, W., Jia, H., Chen, J., 2018. Catalytic combustion of toluene over mesoporous Cr_2O_3-supported platinum catalysts prepared by in situ pyrolysis of MOFs. Chem. Eng. J. 334, 768–779.
Choi, Y.J., Seeley, Z., Bandyopadhyay, A., Bose, S., Akbar, S.A., 2007. Aluminum-doped TiO2 nano-powders for gas sensors. Sens. Actuators B-Chem. 124, 111–117.
Choi, S.W., Katoch, A., Kim, J.H., Kim, S.S., 2014. Prominent reducing gas-sensing performances of n-SnO_2 nanowires by local creation of p-n heterojunctions by functionalization with p-Cr_2O_3 nanoparticles. ACS Appl. Mater. Interfaces 6, 17723–17729.
Chu, C.H., Cheng, S.H., Chen, N.T., Liao, W.N., Lo, L.W., 2019. Microwave-synthesized platinum-embedded mesoporous silica nanoparticles as dual-modality contrast agents: computed tomography and optical imaging. Int. J. Mol. Sci. 20, 1560.
Das, R., Sugimoto, H., Fujii, M., Giri, P.K., 2020. Quantitative understanding of charge-transfer-Mediated Fe^{3+} sensing and fast photoresponse by N-Doped graphene quantum dots decorated on plasmonic Au nanoparticles. ACS Appl. Mater. Interfaces 12, 4755–4768.
Decarolis, D., Lezcano-Gonzalez, I., Gianolio, D., Beale, A.M., 2018. Effect of particle size and support type on Pd catalysts for 1,3-Butadiene hydrogenation. Top. Catal. 61, 162–174.
Deshmane, V.G., Owen, S.L., Abrokwah, R.Y., Kuila, D., 2015. Mesoporous nanocrystalline TiO2 supported metal (Cu, Co, Ni, Pd, Zn, and Sn) catalysts: effect of metal-support interactions on steam reforming of methanol. J. Mol. Catal. A-Chem. 408, 202–213.
Dey, A., 2018. Semiconductor metal oxide gas sensors: a review. Mater. Sci. Eng. B 229, 206–217.
Ding, J., Chan, K.Y., Ren, J.W., Xiao, F.S., 2005. Platinum and platinum-ruthenium nanoparticles supported on ordered mesoporous carbon and their electrocatalytic performance for fuel cell reactions. Electrochim. Acta 50, 3131–3141.
Farmer, J.A., Campbell, C.T., 2010. Ceria maintains smaller metal catalyst particles by strong metal-support bonding. Science 329, 933–936.
Fattakhova-Rohlfing, D., Szeifert, J.M., Yu, Q., Kalousek, V., Rathousky, J., Bein, T., 2009. Low-temperature synthesis of mesoporous titania-silica films with pre-formed anatase nanocrystals. Chem. Mater. 21, 2410–2417.
Fiorenza, R., Spitaleri, L., Gulino, A., Scire, S., 2020. High-performing Au-Ag bimetallic catalysts supported on macro-mesoporous CeO_2 for preferential oxidation of CO in H-2-Rich gases. Catalysts 10, 49.
Gao, Z., Zhang, Y., Li, D., Werth, C.J., Zhang, Y., Zhou, X., 2015. Highly active Pd-In/mesoporous alumina catalyst for nitrate reduction. J. Hazard. Mater. 286, 425–431.
Gates, B.C., Flytzani-Stephanopoulos, M., Dixon, D.A., Katz, A., 2017. Atomically dispersed supported metal catalysts: perspectives and suggestions for future research. Catal. Sci. Technol. 7, 4259–4275.
Gawande, M.B., Goswami, A., Asefa, T., Guo, H., Biradar, A.V., Peng, D.L., Zboril, R., Varma, R.S., 2015. Core-shell nanoparticles: synthesis and applications in catalysis and electrocatalysis. Chem. Soc. Rev. 44, 7540–7590.
Genna, D.T., Wong-Foy, A.G., Matzger, A.J., Sanford, M.S., 2013. Heterogenization of homogeneous catalysts in metal–Organic frameworks via cation exchange. J. Am. Chem. Soc. 135, 10586–10589.
Ghimire, P.P., Zhang, L., Kinga, U.A., Guo, Q., Jiang, B., Jaroniec, M., 2019. Development of nickel-incorporated MCM-41-carbon composites and their application in nitrophenol reduction. J. Mater. Chem. A Mater. Energy Sustain. 7 (16), 9618–9628.
Goncalves, A.A.S., Jaroniec, M., 2019. Evaporation-induced self-assembly synthesis of nanostructured alumina-based mixed metal oxides with tailored porosity. J. Colloid Interface Sci. 537, 725–735.
Goncalves, A.A.S., Faustino, P.B., Assaf, J.M., Jaroniec, M., 2017. One-pot synthesis of mesoporous Ni-Ti-Al ternary oxides: highly active and selective catalysts for steam reforming of ethanol. ACS Appl. Mater. Interfaces 9, 6079–6092.
Goncalves, A.A.S., Costa, M.J.F., Zhang, L., Ciesielczy, F., Jaroniec, M., 2018. One-pot synthesis of $MeAl_2O_4$ (Me = Ni, Co, or Cu) supported on gamma-Al_2O_3 with ultra-large mesopores: enhancing interfacial defects in gamma-Al_2O_3 to facilitate the formation of spinel structures at lower temperatures. Chem. Mater. 30, 436–446.
Grabchenko, M.V., Mamontov, G.V., Zaikovskii, V.I., La Parola, V., Liotta, L.F., Vodyankina, O.V., 2020. The role of metal-support interaction in Ag/CeO_2 catalysts for CO and soot oxidation. Appl. Catal. B-Environ. 260, 118148.
Gu, D., Schüth, F., 2014. Synthesis of non-siliceous mesoporous oxides. Chem. Soc. Rev. 43, 313–344.
Guo, Y., Gu, D., Jin, Z., Du, P.-P., Si, R., Tao, J., Xu, W.-Q., Huang, Y.-Y., Senanayake, S., Song, Q.-S., Jia, C.-J., Schuth, F., 2015. Uniform 2 nm gold nanoparticles supported on iron oxides as active catalysts for CO oxidation reaction: structure-activity relationship. Nanoscale 7, 4920–4928.
Gupta, G., Shah, P.S., Zhang, X., Saunders, A.E., Korgel, B.A., Johnston, K.P., 2005. Enhanced infusion of gold nanocrystals into mesoporous silica with supercritical carbon dioxide. Chem. Mater. 17, 6728–6738.
Gupta, G., Stowell, C.A., Patel, M.N., Gao, X., Yacaman, M.J., Korgel, B.A., Johnston, K.P., 2006. Infusion of presynthesized iridium nanocrystals into mesoporous silica for high catalyst activity. Chem. Mater. 18, 6239–6249.
Guragain, S., Torad, N.L., Alghamdi, Y.G., Alshehri, A.A., Kim, J., Bastakoti, B.P., Yamauchi, Y., 2018. Synthesis of nanoporous calcium carbonate spheres using double hydrophilic block copolymer poly(acrylic acid-b-N-isopropylacrylamide). Mater. Lett. 230, 143–147.
Haruta, M., 2003. When gold is not noble: catalysis by nanoparticles. Chem. Rec. 3, 75–87.
Hayyan, M., Hashim, M.A., AlNashef, I.M., 2016. Superoxide ion: generation and chemical implications. Chem. Rev. 116, 3029–3085.
Huang, W., Kuhn, J.N., Tsung, C.-K., Zhang, Y., Habas, S.E., Yang, P., Somorjai, G.A., 2008. Dendrimer templated synthesis of one nanometer Rh and Pt particles supported on mesoporous silica: catalytic activity for ethylene and pyrrole hydrogenation. Nano Lett. 8, 2027–2034.
Irandoust, A., Haghtalab, A., 2017. A Hybrid reduction-impregnation method in preparation of Co-Ru/gamma-Al_2O_3 Catalyst for Fischer-Tropsch Synthesis. Catal. Lett. 147, 2967–2981.
Ismail, A.A., Bahnemann, D.W., 2011. Mesostructured Pt/TiO_2 nanocomposites as highly active photocatalysts for the photooxidation of dichloroacetic acid. J. Phys. Chem. C 115, 5784–5791.
Ito, Y., Ohta, H., Yamada, Y.M.A., Enoki, T., Uozumi, Y., 2014. Transfer hydrogenation of alkenes using Ni/Ru/Pt/Au heteroquatermetallic nanoparticle catalysts: sequential cooperation of multiple nano-metal species. Chem. Commun. (Camb.) 50, 12123–12126.
Jiang, Y., Gao, Q., 2006. Heterogeneous hydrogenation catalyses over recyclable Pd(0) nanoparticle catalysts stabilized by PAMAM-SBA-15 organic−Inorganic hybrid composites. J. Am. Chem. Soc. 128, 716–717.
Jin, M., Park, J.-N., Shon, J.K., Kim, J.H., Li, Z., Park, Y.K., Kim, J.M., 2012a. Low temperature CO oxidation over Pd catalysts supported on highly ordered mesoporous metal oxides. Catal. Today 185, 183–190.
Jin, Z., Xiao, M., Bao, Z., Wang, P., Wang, J., 2012b. A general approach to mesoporous metal oxide microspheres loaded with noble metal nanoparticles. Angew. Chemie Int. Ed. English 51, 6406–6410.
Jo, J.O., Trinh, Q.H., Kim, S.H., Mok, Y.S., 2018. Plasma-catalytic decomposition of nitrous oxide over gamma-alumina-supported metal oxides. Catal. Today 310, 42–48.
Kale, M.J., Christopher, P., 2016. Utilizing quantitative in situ FTIR spectroscopy to identify well-coordinated Pt atoms as the active site for CO oxidation on Al_2O_3-Supported Pt catalysts. ACS Catal. 6, 5599–5609.
Kamada, K., Fukuda, H., Maehara, K., Yoshida, Y., Nakai, M., Hasuo, S., Matsumoto, Y., 2004. Insertion of SiO_2 nanoparticles into pores of anodized aluminum by electrophoretic deposition in aqueous system. Electrochem. Solid State Lett 7, B25.
Kim, T.-W., Kim, M.-J., Chae, H.-J., Ha, K.-S., Kim, C.-U., 2015. Ordered mesoporous carbon supported uniform rhodium nanoparticles as catalysts for higher alcohol synthesis from syngas. Fuel 160, 393–403.
Konya, Z., Puntes, V.F., Kiricsi, I., Zhu, J., Ager, J.W., Ko, M.K., Frei, H., Alivisatos, P., Somorjai, G.A., 2003. Synthetic insertion of gold nanoparticles into mesoporous silica. Chem. Mater. 15, 1242–1248.
Koo, W.T., Choi, S.J., Kim, S.J., Jang, J.S., Tuller, H.L., Kim, I.D., 2016. Heterogeneous sensitization of metal-organic framework driven Metal@Metal oxide complex catalysts on an oxide nanofiber scaffold toward superior gas sensors. J. Am. Chem. Soc. 138, 13431–13437.
Kresge, C.T., Leonowicz, M.E., Roth, W.J., Vartuli, J.C., Beck, J.S., 1992. Ordered mesoporous molecular sieves synthesized by a liquid-crystal template mechanism. Nature 359, 710–712.
Lang, R., Xi, W., Liu, J.-C., Cui, Y.-T., Li, T., Lee, A.F., Chen, F., Chen, Y., Li, L., Li, L., Lin, J., Miao, S., Liu, X., Wang, A.-Q., Wang, X.-D., Luo, J., Qiao, B., Li, J., Zhang, T., 2019. Non defect-stabilized thermally stable single-atom catalyst. Nat. Commun. 10, 234.
Lewis, R.J., Ueura, K., Fukuta, Y., Freakley, S.J., Kang, L.Q., Wang, R., He, Q., Edwards, J.K., Morgan, D.J., Yamamoto, Y., Hutchings, G.J., 2019. The direct synthesis of H_2O_2 using TS-1 supported catalysts. ChemCatChem 11, 1673–1680.
Li, H., Bian, Z., Zhu, J., Huo, Y., Li, H., Lu, Y., 2007a. Mesoporous Au/TiO_2 nanocomposites with enhanced photocatalytic activity. J. Am. Chem. Soc. 129, 4538–4539.
Li, H., Bian, Z., Zhu, J., Huo, Y., Li, H., Lu, Y., 2007b. Mesoporous Au/TiO_2 nanocomposites with enhanced photocatalytic activity. J. Am. Chem. Soc. 129, 4538–4539.
Li, W., Wu, Z., Wang, J., Elzatahry, A.A., Zhao, D., 2014. A perspective on mesoporous TiO_2 materials. Chem. Mater. 26, 287–298.
Li, Y., Bastakoti, B.P., Yamauchi, Y., 2016. Research Update: Triblock copolymers as templates to synthesize inorganic nanoporous materials. APL Mater. 4, 040703.
Li, J., Song, S., Long, Y., Yao, S., Ge, X., Wu, L., Zhang, Y., Wang, X., Yang, X., Zhang, H., 2018a. A general one-pot strategy for the synthesis of Au@multi-oxide yolk@shell nanospheres with enhanced catalytic performance. Chem. Sci. 9, 7569–7574.
Li, S., Cheng, M., Liu, G., Zhao, L., Zhang, B., Gao, Y., Lu, H., Wang, H., Zhao, J., Liu, F.,

Yan, X., Zhang, T., Lu, G., 2018b. High-response and low-temperature nitrogen dioxide gas sensor based on gold-loaded mesoporous indium trioxide. J Colloid Interf Sci 524, 368–378.
Li, A., Zhu, W., Li, C., Wang, T., Gong, J., 2019. Rational design of yolk-shell nanostructures for photocatalysis. Chem. Soc. Rev. 48, 1874–1907.
Lim, E., Jo, C., Kim, M.S., Kim, M.H., Chun, J., Kim, H., Park, J., Roh, K.C., Kang, K., Yoon, S., Lee, J., 2016. High-performance sodium-ion hybrid supercapacitor based on Nb_2O_5@Carbon core-shell nanoparticles and reduced graphene oxide nanocomposites. Adv. Funct. Mater. 26, 3711–3719.
Lin, C., Compton, R.G., 2017. Size effects in nanoparticle catalysis at nanoparticle modified electrodes: the interplay of diffusion and chemical reactions. J Phys Chem C 121, 2521–2528.
Lin, F.H., Doong, R.A., 2017. Catalytic nanoreactors of Au@Fe_3O_4 yolk-shell nanostructures with various Au sizes for efficient nitroarene reduction. J Phys Chem C 121, 7844–7853.
Liu, J., Zou, S., Li, S., Liao, X., Hong, Y., Xiao, L., Fan, J., 2013. A general synthesis of mesoporous metal oxides with well-dispersed metal nanoparticles via a versatile sol–gel process. J. Mater. Chem. A Mater. Energy Sustain. 1, 4038.
Liu, Q., Joshi, U.A., Uber, K., Regalbuto, J.R., 2014. The control of Pt and Ru nanoparticle size on high surface area supports. Phys. Chem. Chem. Phys. 16, 26431–26435.
Liu, B., Louis, M., Jin, L., Li, G., He, J., 2018. Co-template directed synthesis of gold nanoparticles in mesoporous titanium dioxide. Chem. Eur. J. 24, 9651–9657.
Lohaus, C., Klein, A., Jaegermann, W., 2018. Limitation of Fermi level shifts by polaron defect states in hematite photoelectrodes. Nat. Commun. 9, 4309.
Lu, J., Zhang, P., Li, A., Su, F., Wang, T., Liu, Y., Gong, J., 2013. Mesoporous anatase TiO_2 nanocups with plasmonic metal decoration for highly active visible-light photocatalysis. Chem. Commun. (Camb.) 49, 5817–5819.
Lu, X., Yang, L., Bian, X., Chao, D., Wang, C., 2014. Rapid, Microwave-Assisted, and One-Pot Synthesis of Magnetic Palladium-$CoFe_2O_4$-Graphene Composite Nanosheets and Their Applications as Recyclable Catalysts. Part. Part. Syst. Charact. 31, 245–251.
Lv, X., Chen, J.-F., Tan, Y., Zhang, Y., 2012. A highly dispersed nickel supported catalyst for dry reforming of methane. Catal. Commun. 20, 6–11.
Mccue, J.T., Ying, J.Y., 2007. SnO_2-In_2O_3 nanocomposites as semiconductor gas sensors for CO and NOx detection. Chem. Mater. 19, 1009–1015.
Meixner, H., Gerblinger, J., Lampe, U., Fleischer, M., 1995. Thin-film gas sensors based on semiconducting metal oxides. Sensor Actuat B-Chem 23, 119–125.
Mohammad, N., Bepari, S., Aravamudhan, S., Kuila, D., 2019. Kinetics of fischer-tropsch synthesis in a 3-D printed stainless steel microreactor using different mesoporous silica supported Co-Ru catalysts. Catalysts 9, 872.
Mohammad, N., Abrokwah, R.Y., Steven-Boyd, R.G., Aravamudhan, S., Kuila, D., 2020. Fischer-Tropsch studies in a 3D-printed stainless steel microchannel microreactor coated with cobalt-based bimetallic-MCM-41 catalysts. Catal. Today In Press.
Morris, S.M., Fulvio, P.F., Jaroniec, M., 2008. Ordered mesoporous alumina-supported metal oxides. J. Am. Chem. Soc. 130, 15210–15216.
Muller, S.A., Degler, D., Feldmann, C., Turk, M., Moos, R., Fink, K., Studt, F., Gerthsen, D., Barsan, N., Grunwaldt, J.D., 2018. Exploiting synergies in catalysis and gas sensing using noble metal-loaded oxide composites. ChemCatChem 10, 864–880.
Niu, Z., Li, Y., 2014. Removal and utilization of capping agents in Nanocatalysis. Chem. Mater. 26, 72–83.
Oh, S., Kim, Y.K., Jung, C.H., Doh, W.H., Park, J.Y., 2018. Effect of the metal-support interaction on the activity and selectivity of methanol oxidation over Au supported on mesoporous oxides. Chem. Commun. 54, 8174–8177.
Orilall, M.C., Matsumoto, F., Zhou, Q., Sai, H., Abruna, H.D., DiSalvo, F.J., Wiesner, U., 2009. One-pot synthesis of platinum-based nanoparticles incorporated into mesoporous niobium oxide-carbon composites for fuel cell electrodes. J. Am. Chem. Soc. 131, 9389–9395.
Pacchioni, G., Freund, H.J., 2018. Controlling the charge state of supported nanoparticles in catalysis: lessons from model systems. Chem. Soc. Rev. 47, 8474–8502.
Pacchioni, G., Recart, J.M., Illas, F., 1994. Ab initio cluster model calculations on the chemisorption of CO_2 and SO_2 probe molecules on MgO and CaO (100) surfaces. A Theoretical Measure of Oxide Basicity J Am Chem Soc 116, 10152–10158.
Parra, M.R., Haque, F.Z., 2015. Poly (Ethylene Glycol) (PEG)-assisted shape-controlled synthesis of one-dimensional ZnO nanorods. Optik 126, 1562–1566.
Patel, M.N., Williams, R.D., May, R.A., Uchida, H., Stevenson, K.J., Johnston, K.P., 2008. Electrophoretic deposition of Au nanocrystals inside perpendicular mesochannels of TiO_2. Chemo Mater 20, 6029–6040.
Pillalamarri, S.K., Blum, F.D., Tokuhiro, A.T., Bertino, M.F., 2005. One-pot synthesis of polyaniline - Metal nanocomposites. Chem. Mater. 17, 5941–5944.
Plata, J.J., Graciani, J., Evans, J., Rodriguez, J.A., Sanz, J.F., 2016. Cu deposited on CeOx-Modified TiO2(110): synergistic effects at the metal-oxide interface and the mechanism of the WGS reaction. ACS Catal. 6, 4608–4615.
Ran, J.R., Jaroniec, M., Qiao, S.Z., 2018. Cocatalysts in semiconductor-based photocatalytic CO_2 reduction: achievements, challenges, and opportunities. Adv Mater 30, 1704649.
Ray, C., Pal, T., 2017. Recent advances of metal-metal oxide nanocomposites and their tailored nanostructures in numerous catalytic applications. J. Mater. Chem. A Mater. Energy Sustain. 5, 9465–9487.
Ro, I., Resasco, J., Christopher, P., 2018. Approaches for understanding and controlling interfacial effects in oxide-supported metal catalysts. ACS Catal. 8, 7368–7387.
Rodrigues, T.S., da Silva, A.G.M., Camargo, P.H.C., 2019. Nanocatalysis by noble metal nanoparticles: controlled synthesis for the optimization and understanding of activities. J. Mater. Chem. A Mater. Energy Sustain. 7, 5857–5874.
Rodriguez, J.A., Graciani, J., Evans, J., Park, J.B., Yang, F., Stacchiola, D., Senanayake, S.D., Ma, S.G., Perez, M., Liu, P., Sanz, J.F., Hrbek, J., 2009. Water-gas shift reaction on a highly active inverse CeOx/Cu(111) catalyst: unique role of Ceria nanoparticles. Angew. Chemie Int. Ed. English 48, 8047–8050.
Schrade, A., Landfester, K., Ziener, U., 2013. Pickering-type stabilized nanoparticles by heterophase polymerization. Chem. Soc. Rev. 42 (16), 6823.
Shan, J., Guo, C., Zhu, Y., Chen, S., Song, L., Jaroniec, M., Zheng, Y., Qiao, S.-Z., 2019. Charge-redistribution-Enhanced nanocrystalline Ru@IrO_x electrocatalysts for oxygen evolution in acidic media. Chem 5, 445–459.
Shekhar, M., Wang, J., Lee, W.S., Williams, W.D., Kim, S.M., Stach, E.A., Miller, J.T., Delgass, W.N., Ribeiro, F.H., 2012. Size and support effects for the water-gas shift catalysis over gold nanoparticles supported on model Al_2O_3 and TiO_2. J. Am. Chem. Soc. 134, 4700–4708.
Shen, S., Ding, B., Zhang, S., Qi, X., Wang, K., Tian, J., Yan, Y., Ge, Y., Wu, L., 2017. Near-infrared light-responsive nanoparticles with thermosensitive yolk-shell structure for multimodal imaging and chemo-photothermal therapy of tumor. NanomedNanotechnol 13, 1607–1616.
Shen, Y., Li, Q., Li, T., Cao, M., Gu, F., Wang, L., Zhu, D.-M., 2020. Improved ethanol gas-sensing properties of optimum Fe-ZnO mesoporous nanoparticles. J Mater Sci-Mater El 31, 3074–3083.
Shim, J., Lee, J., Ye, Y., Hwang, J., Kim, S.K., Lim, T.H., Wiesner, U., Lee, J., 2012. One-pot synthesis of intermetallic electrocatalysts in ordered, large-pore mesoporous Carbon/Silica toward formic acid oxidation. ACS Nano 6, 6870–6881.
Skrabalak, S.E., Xia, Y., 2009. Pushing nanocrystal synthesis toward nanomanufacturing. ACS Nano 3, 10–15.
Solovyeva, V.A., Vu, K.B., Merican, Z., Sougrat, R., Rodionov, V.O., 2014. One-pot synthesis of Au@SiO_2 catalysts: a click chemistry approach. ACS Comb. Sci. 16, 513–517.
Song, S., Wang, X., Zhang, H., 2015. CeO_2-encapsulated noble metal nanocatalysts: enhanced activity and stability for catalytic application. NPG Asia Mater. 7, e179.
Stavale, F., Shao, X., Nilius, N., Freund, H.J., Prada, S., Giordano, L., Pacchioni, G., 2012. Donor characteristics of transition-metal-Doped oxides: Cr-Doped MgO versus Mo-Doped CaO. J. Am. Chem. Soc. 134, 11380–11383.
Sterrer, M., Yulikov, M., Fischbach, E., Heyde, M., Rust, H.P., Pacchioni, G., Risse, T., Freund, H.J., 2006. Interaction of gold clusters with color centers on MgO(001) films. Angew. Chemie Int. Ed. English 45, 2630–2632.
Sun, Y., Xia, Y., 2002. Shape-controlled synthesis of gold and silver nanoparticles. Science 298, 2176–2179.
Sun, S., Wang, W., Zeng, S., Shang, M., Zhang, L., 2010. Preparation of ordered mesoporous Ag/WO_3 and its highly efficient degradation of acetaldehyde under visible-light irradiation. J. Hazard. Mater. 178, 427–433.
Suttiponparnit, K., Jiang, J.K., Sahu, M., Suvachittanont, S., Charinpanitkul, T., Biswas, P., 2011. Role of surface area, primary particle size, and crystal phase on titanium dioxide nanoparticle dispersion properties. Nanoscale Res. Lett. 6, 27.
Tadros, T., 2012. Electrostatic and Steric Stabilization of Colloidal Dispersions. John Willey & Sons, Hoboken, NJ, pp. 153–172.
Talebzadeh, S., Queffelec, C., Knight, D.A., 2019. Surface modification of plasmonic noble metal-metal oxide core-shell nanoparticles. Nanoscale Adv. 1, 4578–4591.
Tao, F., Grass, M.E., Zhang, Y., Butcher, D.R., Renzas, J.R., Liu, Z., Chung, J.Y., Mun, B.S., Salmeron, M., Somorjai, G.A., 2008. Reaction-driven restructuring of Rh-Pd and Pt-Pd core-shell nanoparticles. Science 322, 932–934.
Tauster, S.J., Fung, S.C., Garten, R.L., 1978. Strong metal-support interactions. Group 8 noble metals supported on titanium dioxide. J. Am. Chem. Soc. 100, 170–175.
Tian, Y., Qi, J., Zhang, W., Cai, Q., Jiang, X., 2014. Facile, One-Pot Synthesis, and Antibacterial Activity of Mesoporous Silica Nanoparticles Decorated with Well-Dispersed Silver Nanoparticles. ACS Appl. Mater. Interfaces 6, 12038–12045.
Tomer, V.K., Adhyapak, P.V., Duhan, S., Mulla, I.S., 2014. Humidity sensing properties of Ag-loaded mesoporous silica SBA-15 nanocomposites prepared via hydrothermal process. Microporous Mesoporous Mater. 197, 140–147.
van Deelen, T.W., Mejia, C.H., de Jong, K.P., 2019. Control of metal-support interactions in heterogeneous catalysts to enhance activity and selectivity. Nat. Catal. 2, 955–970.
Vayssilov, G.N., Lykhach, Y., Migani, A., Staudt, T., Petrova, G.P., Tsud, N., Skala, T., Bruix, A., Illas, F., Prince, K.C., Matolin, V., Neyman, K.M., Libuda, J., 2011. Support nanostructure boosts oxygen transfer to catalytically active platinum nanoparticles. Nat. Mater. 10, 310–315.
Wang, G., Ji, Y., Huang, X., Yang, X., Gouma, P.I., Dudley, M., 2006. Fabrication and characterization of polycrystalline WO_3 nanofibers and their application for ammonia sensing. J. Phys. Chem. B 110, 23777–23782.
Wang, Z., Xie, Y., Liu, C., 2008a. Synthesis and characterization of noble metal (Pd, Pt, Au, Ag) nanostructured materials confined in the channels of mesoporous SBA-15. J. Phys. Chem. C 112, 19818–19824.
Wang, L.-C., Huang, C.-Y., Chang, C.-Y., Lin, W.-C., Chao, K.-J., 2008b. Formation of Pd nanoparticles in surfactant-mesoporous silica composites and surfactant solutions. Microporous Mesoporous Mater. 110, 451–460.
Wang, H., Jeong, H.Y., Imura, M., Wang, L., Radhakrishnan, L., Fujita, N., Castle, T., Terasaki, O., Yamauchi, Y., 2011. Shape- and size-controlled synthesis in hard templates: sophisticated chemical reduction for mesoporous monocrystalline platinum nanoparticles. J. Am. Chem. Soc. 133, 14526–14529.
Wang, J., Lu, A.-H., Li, M., Zhang, W., Chen, Y.-S., Tian, D.-X., Li, W.-C., 2013. Thin porous alumina sheets as supports for stabilizing gold nanoparticles. ACS Nano 7, 4902–4910.
Wang, F.F., Shao, S., Liu, C.L., Xu, C.L., Yang, R.Z., Dong, W.S., 2015. Selective oxidation of glycerol over Pt supported on mesoporous carbon nitride in base-free aqueous solution. Chem. Eng. J. 264, 336–343.
Wang, M., Zhang, Q., Zhang, T., Wang, Y., Wang, J., Long, K., Song, Z., Liu, X., Ning, P., 2017a. Facile one-pot synthesis of highly dispersed Ni nanoparticles embedded in HMS for dry reforming of methane. Chem. Eng. J. 313, 1370–1381.
Wang, Y., Liu, J., Cui, X., Gao, Y., Ma, J., Sun, Y., Sun, P., Liu, F., Liang, X., Zhang, T., Lu, G., 2017b. NH_3gas sensing performance enhanced by Pt-loaded on mesoporous WO_3. Sens. Actuators B-Chem. 238, 473–481.

Wang, Z., He, B., Xu, G., Wang, G., Wang, J., Feng, Y., Su, D., Chen, B., Li, H., Wu, Z., Zhang, H., Shao, L., Chen, H., 2018. Transformable masks for colloidal nanosynthesis. Nat. Commun. 9, 563.
Wei, B., Sheng, K., Ge, J., 2018. Internally supported metal-oxide nanocatalyst for hydrogenation of nitroaromatics. Langmuir 34, 7077–7085.
Wen, C., Zhu, Y., Ye, Y., Zhang, S., Cheng, F., Liu, Y., Wang, P., Tao, F., 2012. Water–Gas shift reaction on metal nanoclusters encapsulated in mesoporous Ceria Studied with ambient-pressure X-ray photoelectron spectroscopy. ACS Nano 6, 9305–9313.
Winterbo, W.l, 1967. Equilibrium shape of a small particle in contact with a foreign substrate. Acta Metall. Mater. 15, 303–310.
Witzke, M.E., Dietrich, P.J., Ibrahim, M.Y.S., Al-Bardan, K., Triezenberg, M.D., Flaherty, D.W., 2017. Spectroscopic evidence for origins of size and support effects on selectivity of Cu nanoparticle dehydrogenation catalysts. Chem. Commun. 53, 597–600.
Wong, K., Zeng, Q.H., Yu, A.B., 2011. Electronic structure of metal (M = Au, Pt, Pd, or Ru) bilayer modified α-Fe_2O_3(0001) surfaces. J. Phys. Chem. C 115, 4656–4663.
Xu, D., Lv, H., Liu, B., 2018. Encapsulation of metal nanoparticle catalysts within mesoporous zeolites and their enhanced catalytic performances: a review. Front. Chem. 6, 550.
Xu, X., Megarajan, S.K., Zhang, Y., Jiang, H., 2020. Ordered mesoporous alumina and their composites based on evaporation induced self-assembly for adsorption and catalysis. Chem. Mater. 32, 3–26.
Yadav, R., Singh, H., Sinha, A.K., 2019. Ultra-fine size-controlled Pt (111) nanoparticles supported on mesoporous titania as an efficient photoelectrocatalyst for hydrogen evolution. Appl. Surf. Sci. 495, 143525.
Yamazoe, N., Kurokawa, Y., Seiyama, T., 1983. Effects of additives on semiconductor gas sensors. Sens. Actuators 4, 283–289.
Yan, Z., Xu, Z., Yu, J., Jaroniec, M., 2015. Highly active mesoporous ferrihydrite supported Pt catalyst for formaldehyde removal at room temperature. Environ. Sci. Technol. 49, 6637–6644.
Yanagisawa, T., Shimizu, T., Kuroda, K., Kato, C., 1990. The preparation of alkyltrimethylammonium-kanemite complexes and their conversion to microporous materials. Bull. Chem. Soc. Jpn. 63, 988–992.
Yang, L.Y., Li, H.Z., Liu, J., Sun, Z.Q., Tang, S.S., Lei, M., 2015. Dual yolk-shell structure of carbon and silica-coated silicon for high-performance lithium-ion batteries. Sci. Rep. 5, 10908.
Yang, T., Ling, H., Lamonier, J.-F., Jaroniec, M., Huang, J., Monteiro, M.J., Liu, J., 2016. A synthetic strategy for carbon nanospheres impregnated with highly monodispersed metal nanoparticles. NPG Asia Mater. 8, e240.
Yang, Q., Xu, Q., Jiang, H.L., 2017. Metal-organic frameworks meet metal nanoparticles: synergistic effect for enhanced catalysis. Chem. Soc. Rev. 46, 4774–4808.
Yao, Q., Lu, Z.-H., Zhang, Z., Chen, X., Lan, Y., 2014. One-pot synthesis of core-shell Cu@SiO_2 nanospheres and their catalysis for hydrolytic dehydrogenation of ammonia borane and hydrazine borane. Sci. Rep. 4, 7597.
Yi, X., Guo, D., Li, P., Lian, X., Xu, Y., Dong, Y., Lai, W., Fang, W., 2017. One pot synthesis of NiMo-Al_2O_3 catalysts by solvent-free solid-state method for hydrodesulfurization. RSC Adv. 7, 54468–54474.
Yuan, Q., Duan, H.-H., Li, L.-L., Li, Z.-X., Duan, W.-T., Zhang, L.-S., Song, W.-G., Yan, C.-H., 2010. Homogeneously dispersed Ceria nanocatalyst stabilized with ordered mesoporous alumina. Adv. Mater. 22, 1475–1478.
Zalduendo, M.M., Langer, J., Giner-Casares, J.J., Halac, E.B., Soler-Illia, G.J.A.A., Liz-Marzan, L.M., Angelome, P.C., 2018. Au nanoparticles-mesoporous TiO2 thin films composites as SERS sensors: a systematic performance analysis. J. Phys. Chem. C 122, 13095–13105.
Zhang, L., Shen, Y., 2015. One-pot synthesis of Platinum-Ceria/Graphene nanosheet as advanced electrocatalysts for alcohol oxidation. Chemelectrochem 2, 887–895.
Zhang, Q., Wang, H., 2014. Facet-dependent catalytic activities of Au nanoparticles enclosed by high-index facets. ACS Catal. 4, 4027–4033.
Zhang, L., Jin, L., Liu, B., He, J., 2019a. Templated growth of crystalline mesoporous materials: from Soft/Hard templates to colloidal templates. Front. Chem. 7, 22.
Zhang, L., Filot, I.A.W., Su, Y.-Q., Liu, J.-X., Hensen, E.J.M., 2019b. Understanding the impact of defects on catalytic CO oxidation of LaFeO3-Supported Rh, Pd, and Pt single-atom catalysts. J. Phys. Chem. C 123, 7290–7298.
Zhang, L.P., Goncalves, A.A.S., Jiang, B., Jaroniec, M., 2020a. A generalized strategy for synthesizing crystalline bismuth-containing nanomaterials. Nanoscale 12, 8277–8284.
Zhang, B., Zhang, J., Lin, Y., Liu, M., Fang, G., Wang, S., 2020b. Coral-like Au_1Pt_3 alloy nanoparticles with multiple surface defects modified by poly(L-methionine) membrane for the selective detection of dopamine in biological samples. J. Alloys Compd. 815, 152643.
Zhao, S., Nagineni, V.S., Seetala, N.V., Kuila, D., 2008. Microreactors for syngas conversion to higher alkanes: effect of ruthenium on silica-supported iron-cobalt nanocatalysts. Ind. Eng. Chem. Res. 47, 1684–1688.
Zheng, N., Stucky, G.D., 2006. A general synthetic strategy for oxide-supported metal nanoparticle catalysts. J. Am. Chem. Soc. 128, 14278–14280.
Zheng, Y., Vasileff, A., Zhou, X., Jiao, Y., Jaroniec, M., Qiao, S.-Z., 2019. Understanding the roadmap for electrochemical reduction of CO_2 to multi-carbon oxygenates and hydrocarbons on copper-based catalysts. J. Am. Chem. Soc. 14, 7646–7659.
Zhong, Q., Cao, M., Hu, H., Yang, D., Chen, M., Li, P., Wu, L., Zhang, Q., 2018. One-pot synthesis of highly stable $CsPbBr_3$@SiO_2 core-shell nanoparticles. ACS Nano 12, 8579–8587.